SIAM/ASA J. Uncertainty Quantification
Vol. 3, pp. 169–198

A Posteriori Error Estimates for Mixed Finite Element and Finite Volume Methods for Parabolic Problems Coupled through a Boundary*

T. Arbogast†, D. Estep‡, B. Sheehan§, and S. Tavener§

Abstract. We examine two discretization schemes for solving a pair of parabolic problems with significantly different spatial and temporal scales that are coupled through a common interface: a mixed finite element method which uses a rigorous mortar element technique in both space and time for coupling and a finite volume method which employs popular ad hoc projections for coupling. We derive a posteriori error estimates to quantify the distinct sources of error for both methods as well as discuss implementation of the estimates. The estimates include expressions that quantify the effects of using a finite number of iterations when solving the discrete equations yielding the approximations. We use the estimates to investigate the consequences of particular discretization choices on the accuracy of the computations.

Key words. mortar methods, a posteriori error estimate, coupled elliptic problems, heterogeneous domain decomposition, geometric coupling, iteration error

AMS subject classifications. 65M08, 65M15, 65M60, 65M22

DOI. 10.1137/140964059

1. Introduction.

In a common class of multiscale, multiphysics problems, two physical processes with distinct spatial and temporal scales are posed in neighboring subdomains and their solutions are coupled by continuity of state and normal flux through their shared boundary. Examples include general problems of the heterogeneous domain decomposition type [30, 23, 6], core-edge plasma simulations of a tokamak fusion experiment [10, 11], and conjugate heat transfer between a fluid and solid object [19, 20, 21].

Significant differences in spatial and temporal scales indicate the use of different discretization grids and time steps in the two subdomains, which raises the problem of transferring

*Received by the editors April 7, 2014; accepted for publication (in revised form) December 30, 2014; published electronically February 26, 2015.

http://www.siam.org/journals/juq/3/96405.html

†Department of Mathematics, University of Texas at Austin, Austin, TX 78712 (arbogast@math.utexas.edu). This author's work was supported as part of the Center for Frontiers of Subsurface Energy Security, an Energy Frontier Research Center funded by the U.S. Department of Energy, Office of Science, Office of Basic Energy Sciences under award DE-SC0001114.

‡Department of Statistics, Colorado State University, Fort Collins, CO 80523 (estep@stat.colostate.edu). This author's work was supported in part by the Defense Threat Reduction Agency (HDTRA1-09-1-0036), the Department of Energy (DE-FG02-04ER25620, DE-FG02-05ER25699, DE-FC02-07ER54909, DE-SC0001724, DE-SC0005304, INL00120133, DE0000000SC9279), Idaho National Laboratory (00069249, 00115474), Lawrence Livermore National Laboratory (B584647, B590495), the National Science Foundation (DMS-0107832, DMS-0715135, DGE-0221595003, MSPA-CSE-0434354, ECCS-0700559, DMS-1065046, DMS-1016268, DMS-FRG-1065046), and the National Institutes of Health (R01GM096192).

§Department of Mathematics, Colorado State University, Fort Collins, CO 80523 (brendansheehan6@gmail.com, tavener@math.colostate.edu). The third author's work was supported in part by the Department of Energy (DE-FG02-04ER25620). The fourth author's work was supported in part by the Department of Energy (DE-FG02-04ER25620, INL00120133) and the National Science Foundation (DMS-1016268).

the coupling quantities between the different discretizations [19, 20, 21, 22]. Moreover, the discrete systems yielding the approximate solution are difficult to solve and generally require an iterative approach. Often, decisions regarding the numerical solution of such coupled systems are made largely based on considerations of data structures, parallel computing, and properties of legacy codes rather than achieving optimal convergence [29]. This is rationalized by assuming that for coupled parabolic problems, coupling has minimal impact on the stability and accuracy and accuracy can be maintained even when iterative solvers stop well short of convergence.

In fact, the choice of coupling method, iterative solution technique, and the number of iterations employed all have a strong impact on the accuracy and stability of the approximation [29]. In our experience, numerical error in the solution of coupled systems is nearly always significant. Unfortunately, a priori error analysis generally leads to a pessimistic conclusion that requires either severe time step constraints or a large number of iterations. This provides strong motivation for deriving a posteriori error estimates that accurately quantify the effects of numerical solution of the components, coupling, and finite iteration on accuracy. Moreover, accurate computational error estimation is also a key component of uncertainty quantification for coupled systems because numerical error introduces significant bias in stochastic computations; see, e.g., [16, 17, 9], which present a posteriori error analysis for approximate cumulative distribution functions and p-quantiles computed from differential equations with stochastic parameters.

In this paper we address the derivation and implementation of a posteriori error estimates for two different discretization schemes for solving a pair of parabolic problems with distinct spatial and temporal scales that are coupled across a common interface. The first is a mixed finite element method using a mortar element technique to couple the subdomains, while the second discretization is a finite volume method using somewhat ad hoc projections to exchange information across the interface. The mortar element approach [8, 31, 1, 5, 3, 24, 2] is based on a rigorous variational formulation to define a weak sense of coupling. The second approach employs "geometric" extrapolation and averaging commonly encountered in practice. We use a posteriori error analysis employing computable residuals, solutions of adjoint problems, and variational analysis to obtain reliably accurate estimates of the error in a given quantity of interest [15, 4, 25, 34, 2, 18, 27].

The analysis in this paper extends [2], which treats these approaches for stationary problems, in order to address coupled nonlinear parabolic problems. To wit, this paper

1. extends the mortar element and "geometric" ad hoc coupling techniques to time dependent problems,
2. formulates two iterative techniques for solving the discrete equations arising at each time step,
3. extends the a posteriori analysis to nonlinear time dependent problems,
4. extends the a posteriori analysis to include the effects arising from finite iteration of these iterative schemes, and
5. addresses issues involved in numerical solution of the adjoint problem.

We use the error estimates to investigate the consequences of particular discretization choices. Since the effects of various spatial discretization choices were thoroughly investigated in [2], we concentrate on the new issues arising due to time discretization.

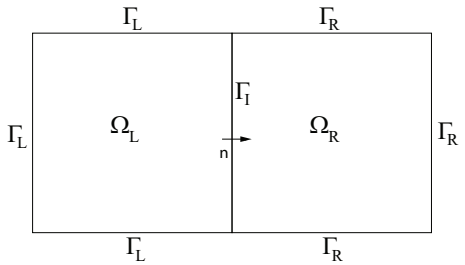

Figure 1. *The spatial domain and definition of normal* $\boldsymbol{n}$ *on the interface.*

The remainder of this paper is organized as follows. Section 2 introduces the continuous problem, provides details of the two discretization methods, and develops two different iterative methods to solve the resulting discrete systems. Section 3 presents the a posteriori error estimates, and section 4 contains the numerical experiments. Section 5 contains proofs justifying the estimates in section 3. We draw conclusions in section 6.

2. Problem definition and discretization methods. We employ the well-known equivalence between finite volume methods and the mixed finite element method [26, 32, 33] to recast all of the discretizations in the finite element framework. This enables the derivation of a posteriori error estimates and provides a systematic framework for describing geometric approaches to computing coupling values.

2.1. The model problem. We consider a system of second order parabolic partial differential equations (PDEs) posed on a rectangular domain $\Omega = \Omega_L \cup \Omega_R$ consisting of two nonoverlapping rectangular subdomains Ω_L and Ω_R that share an interface along a common side $\Gamma_I = \bar{\Omega}_L \cap \bar{\Omega}_R$; see Figure 1. The unit normal vector $\boldsymbol{n}$ on Γ_I points from Ω_L to Ω_R. We let $\Gamma_L = \partial\Omega_L \setminus \Gamma_I$ and $\Gamma_R = \partial\Omega_R \setminus \Gamma_I$ denote the outer boundaries of the subdomains. For simplicity, we assume Dirichlet boundary conditions on $\partial\Omega$ and write out details in the homogeneous case. The results extend to problems with other boundary conditions in a straightforward way.

To define the PDE, we pose source functions $f \in L^2(L^2(\Omega); (0,T])$ and $g \in L^\infty(\mathbb{R})$ and initial data $p_0 \in L^2(\Omega)$. For a function φ, we use the notation $\varphi_L = \varphi|_{\Omega_L}$ and $\varphi_R = \varphi|_{\Omega_R}$, so the boundary data d is $d_L \in L^2(H^{3/2}(\Gamma_L); (0,T])$ and $d_R \in L^2(H^{3/2}(\Gamma_R); (0,T])$. The coupled system is

$$\begin{cases} a_L^{-1}\boldsymbol{u}_L + \nabla p_L = 0, & (x,y) \in \Omega_L, t \in (0,T], \\ \dot{p}_L + \nabla \cdot \boldsymbol{u}_L = f_L + g_L(p_L), & (x,y) \in \Omega_L, t \in (0,T], \\ p_L = d_L, & (x,y) \in \Gamma_L, t \in (0,T], \\ p_L = p_{0,L}, & (x,y) \in \Omega_L, t = 0, \end{cases} \tag{2.1}$$

$$\begin{cases} a_R^{-1}\boldsymbol{u}_R + \nabla p_R = 0, & (x,y) \in \Omega_R, t \in (0,T], \\ \dot{p}_R + \nabla \cdot \boldsymbol{u}_R = f_R + g_R(p_R), & (x,y) \in \Omega_R, t \in (0,T], \\ p_R = d_R, & (x,y) \in \Gamma_R, t \in (0,T], \\ p_R = p_{0,R}, & (x,y) \in \Omega_R, t = 0, \end{cases} \tag{2.2}$$

$$\begin{cases} \xi \equiv p_L = p_R, & (x,y) \in \Gamma_I, t \in (0,T], \\ \boldsymbol{n} \cdot (\boldsymbol{u}_L - \boldsymbol{u}_R) = 0, & (x,y) \in \Gamma_I, t \in (0,T], \end{cases} \tag{2.3}$$

where a is a diagonal diffusion matrix defined as

$$a_i = \begin{bmatrix} D_i(x,y,t) & 0 \\ 0 & D_i(x,y,t) \end{bmatrix}, \quad i = L, R, \tag{2.4}$$

with $D_i \in W^{1,\infty}(\Omega)$ and $D_i(x,y,t) \geq D_0 > 0$ for $(x,y,t) \in \overline{\Omega}$. So, a_i is invertible and uniformly coercive. Note that ξ is the common interface pressure in (2.3). We also assume that f, g, d, p_0, and a are continuous in the subdomains.

2.2. A variational formulation. We abuse notation slightly to define the L^2 inner product on Ω by restriction to the subdomains, i.e., for functions F and G defined on Ω with restrictions F_i, G_i on Ω_i, $i = L, R$,

$$(F_i, G_i) = \int_{\Omega_i} F_i(x,y)\, G_i(x,y)\, \mathrm{d}x\, \mathrm{d}y, \quad i = L, R.$$

For functions F, G on boundaries, we define

$$\langle F, G \rangle_{\Gamma_i} = \int_{\Gamma_i} F\, G\, \mathrm{d}s, \quad i = L, I, R.$$

The weak formulation is as follows: Find $p_i \in W_i = L^2(L^2(\Omega_i); (0,T])$, $\boldsymbol{u}_i \in \boldsymbol{V}_i = L^2(H(\mathrm{div}; \Omega_i), (0,T])$, $\xi \in \Lambda = L^2(H^{1/2}(\Gamma_I), (0,T])$, $i = L, R$, satisfying

$$\begin{aligned}
&\int_0^T (a_L^{-1} \boldsymbol{u}_L, \boldsymbol{v}_L)\, \mathrm{d}t - \int_0^T (p_L, \nabla \cdot \boldsymbol{v}_L)\, \mathrm{d}t + \int_0^T \langle \xi, \boldsymbol{n} \cdot \boldsymbol{v}_L \rangle_{\Gamma_I}\, \mathrm{d}t = -\int_0^T \langle d_L, \boldsymbol{n} \cdot \boldsymbol{v}_L \rangle_{\Gamma_L}\, \mathrm{d}t, \\
&\int_0^T (\dot{p}_L, w_L)\, \mathrm{d}t + \int_0^T (\nabla \cdot \boldsymbol{u}_L, w_L)\, \mathrm{d}t = \int_0^T (f_L, w_L)\, \mathrm{d}t + \int_0^T (g_L(p_L), w_L)\, \mathrm{d}t, \\
&\int_0^T (a_R^{-1} \boldsymbol{u}_R, \boldsymbol{v}_R)\, \mathrm{d}t - \int_0^T (p_R, \nabla \cdot \boldsymbol{v}_R)\, \mathrm{d}t - \int_0^T \langle \xi, \boldsymbol{n} \cdot \boldsymbol{v}_R \rangle_{\Gamma_I}\, \mathrm{d}t = -\int_0^T \langle d_R, \boldsymbol{n} \cdot \boldsymbol{v}_R \rangle_{\Gamma_R}\, \mathrm{d}t, \\
&\int_0^T (\dot{p}_R, w_R)\, \mathrm{d}t + \int_0^T (\nabla \cdot \boldsymbol{u}_R, w_R)\, \mathrm{d}t = \int_0^T (f_R, w_R)\, \mathrm{d}t + \int_0^T (g_R(p_R), w_R)\, \mathrm{d}t, \\
&\int_0^T \langle \boldsymbol{n} \cdot (\boldsymbol{u}_L - \boldsymbol{u}_R), \nu \rangle_{\Gamma_I}\, \mathrm{d}t = 0
\end{aligned} \tag{2.5}$$

for all $(w_i, \boldsymbol{v}_i, \nu) \in (W_i, \boldsymbol{V}_i, \Lambda)$, $i = L, R$.

2.3. Mortar mixed finite element discretization. It is necessary to devise a coupling scheme to transfer information, e.g., normal flux and states, between the discretizations of the two components. The traditional mortar finite element approach for a stationary problem uses an auxiliary variable supported on the interface to achieve coupling that has certain optimal properties with respect to approximation accuracy. We construct a mortar finite element method in space and time.

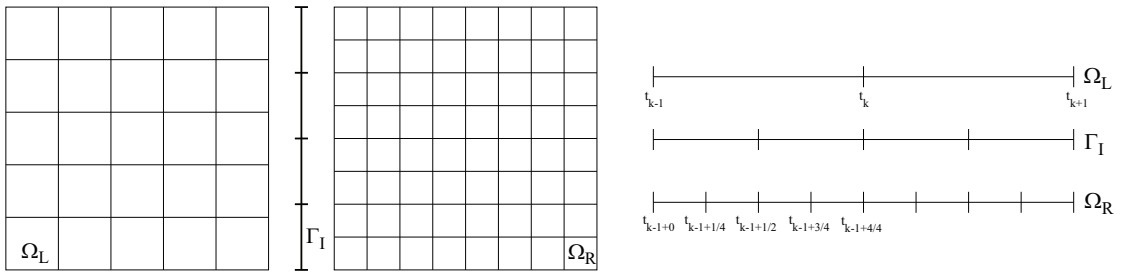

Figure 2. *The left half of the figure shows the spatial grids on Ω_L, Γ_I, and Ω_R. The right half of the figure shows the corresponding time discretizations.*

We partition Ω_i by a rectangular grid $\mathcal{T}_{h_i}$ of nonoverlapping uniform-shaped cells of size h_i such that the union of the cells is Ω_i, $i = L, R$. The discretization grids for Ω_L and Ω_R may be different. We construct a grid on Γ_I such that the spatial cell width on the interface grid, h_Γ, is twice the cell width of the finer of the two component grids ($h_\Gamma = 2\min\{h_L, h_R\}$).

For each Ω_i, we construct a time discretization of $[0, T]$ into time nodes, with a coarser grid associated with Ω_L and a finer grid associated with Ω_R such that each large time step on the coarse grid is divided into an integer number of substeps on the finer grid [28]. The coarse grid time nodes thus act as "synchronization" times. The coarse time step intervals are denoted by $I_k = [t_{k-1}, t_k]$, $k = 1, \ldots, n$. A fractional index is used to denote the subintervals on the fine scale, so that for $j = 1, \ldots, q$ the small subintervals are $I_{k+j/q} = [t_{k-1+\frac{j-1}{q}}, t_{k-1+\frac{j}{q}}]$, where q is the number of substeps in each coarse time step. We also associate a discretization of $[0, T]$ with Γ_I constructed so that the cell width in time on the interface is twice that of the finer of the two component time steps and is a subdivision of the coarser time discretization. We suppress the notation for the time steps on the interface. A single time step on the coarse side together with the associated substeps on the fine side and interface is called a composite time step. We illustrate this in Figure 2.

To discretize in space, we use the lowest order Raviart–Thomas finite element space ($RT0$), in which the discrete scalar unknown p^h is approximated as a constant over each cell, and the components of the discrete vector $\boldsymbol{u}^h$ are approximated by functions that are piecewise linear in one spatial dimension and constant in the other [7, 18]. On the interface, the discrete interface unknown, ξ^h, is represented by piecewise discontinuous bilinears on the space-time interface grid cells [1, 3].

To discretize in time, we use the lowest order discontinuous Galerkin finite element space (DG0) [15]. The approximate solution is a piecewise constant function with respect to the time discretization, so the approximate p is specified as $p_L^h|_{I_k} = p_L^{h,k}$ and $p_R^h|_{I_k+j/q} = p_L^{h,k+j/q}$. The test functions are also piecewise constant with respect to the time discretization. This generally simplifies the evaluation of the time integrals in the weak formulation, except that discontinuities at time nodes yield "jump terms" arising from the time derivative, e.g.,

$$\int_0^T (\dot{p}_L^h, w)\,\mathrm{d}t = \sum_{k=1}^{n} \int_{t_{k-1}}^{t_k} (\dot{p}_L^h, w)\,\mathrm{d}t + \sum_{k=1}^{n} ([(p_L^h)_{k-1}], w_{k-1}), \tag{2.6}$$

where $[p_k] = p_k^+ - p_k^-$, $p_k^{+/-} = \lim_{s \to t_k^{+/-}} p(\mathbf{x}, s)$, $w_k = w_k^+$. Note that $\int_{t_{k-1}}^{t_k} (\dot{p}_L^h, w)\,\mathrm{d}t$ vanishes for DG0; however, we keep this term in the weak forms below for generality.

The DG0 method is an implicit method closely related to the backward Euler scheme. The use of implicit schemes for the time solution of each component is common in practice. It is possible to treat explicit schemes; see, e.g., [12]. However, explicit discretization introduces additional effects on stability and accuracy that must be treated in the analysis, and we avoid this here for simplicity.

On the interface, for a finite element partition Δ of $[a, b]$, and for $r = 0, 1, 2, \ldots$, $q = -1, 0, 1, \ldots$, we define the piecewise polynomial space

$$\mathcal{M}_q^r(\Delta) = \{v \in C^q([a, b]) : v \text{ a polynomial of degree } \leq r \text{ on each subinterval of } \Delta\}.$$

When $q = -1$, the functions are discontinuous. The space of continuous piecewise bilinear functions is the tensor product $\mathcal{M}_0^1(\Delta_x) \otimes \mathcal{M}_0^1(\Delta_y)$. The $RT0 \times DG0$ discrete spaces are

$$W_i^h = \mathcal{M}_{-1}^0(\Delta_{x,i}) \otimes \mathcal{M}_{-1}^0(\Delta_{y,i}) \otimes \mathcal{M}_{-1}^0(\Delta_{t,i}),$$
$$\boldsymbol{V}_i^h = [\mathcal{M}_0^1(\Delta_{x,i}) \otimes \mathcal{M}_{-1}^0(\Delta_{y,i}) \otimes \mathcal{M}_{-1}^0(\Delta_{t,i})] \times [\mathcal{M}_{-1}^0(\Delta_{x,i}) \otimes \mathcal{M}_0^1(\Delta_{y,i}) \otimes \mathcal{M}_{-1}^0(\Delta_{t,i})],$$
$$\Lambda^h = \mathcal{M}_{-1}^1(\Delta_{\Gamma_I}) \otimes \mathcal{M}_{-1}^1(\Delta_{t,i})(\Delta_{\Gamma_I})$$

for $i = L, R$. We suppress the superscript denoting the time interval when writing time integrals. The mortar mixed finite element method reads as follows: For $k = 1, 2, \ldots$, compute $p_i^h \in W_i^h$, $\boldsymbol{u}_i^h \in \boldsymbol{V}_i^h$, $\xi^h \in \Lambda^h$, $i = L, R$, satisfying

$$\int_{t_{k-1}}^{t_k} (a_L^{-1}\boldsymbol{u}_L^h, \boldsymbol{v}_L)\,\mathrm{d}t - \int_{t_{k-1}}^{t_k} (p_L^h, \nabla \cdot \boldsymbol{v}_L)\,\mathrm{d}t + \int_{t_{k-1}}^{t_k} \langle \xi^h, \boldsymbol{n} \cdot \boldsymbol{v}_L \rangle_{\Gamma_I}\,\mathrm{d}t = -\int_{t_{k-1}}^{t_k} \langle d_L, \boldsymbol{n} \cdot \boldsymbol{v}_L \rangle_{\Gamma_L}\,\mathrm{d}t,$$

$$\int_{t_{k-1}}^{t_k} (\dot{p}_L^h, w_L)\,\mathrm{d}t + ([p_{L,k-1}^h], w_{L,k-1}) + \int_{t_{k-1}}^{t_k} (\nabla \cdot \boldsymbol{u}_L^h, w_L)\,\mathrm{d}t$$
$$= \int_{t_{k-1}}^{t_k} (f_L, w_L)\,\mathrm{d}t + \int_{t_{k-1}}^{t_k} (g_L(p_L^h), w_L)\,\mathrm{d}t,$$

$$\int_{t_{k-1}}^{t_k} (a_R^{-1}\boldsymbol{u}_R^h, \boldsymbol{v}_R)\,\mathrm{d}t - \int_{t_{k-1}}^{t_k} (p_R^h, \nabla \cdot \boldsymbol{v}_R)\,\mathrm{d}t - \int_{t_{k-1}}^{t_k} \langle \xi^h, \boldsymbol{n} \cdot \boldsymbol{v}_R \rangle_{\Gamma_I}\,\mathrm{d}t = -\int_{t_{k-1}}^{t_k} \langle d_R, \boldsymbol{n} \cdot \boldsymbol{v}_R \rangle_{\Gamma_R}\,\mathrm{d}t,$$

$$\sum_{j=1}^{q} \int_{t_{k-1+\frac{j-1}{q}}^+}^{t_{k-1+\frac{j}{q}}^-} (\dot{p}_R^h, w_R)\,\mathrm{d}t + \sum_{j=1}^{q} ([p_{R,k-1+\frac{j-1}{q}}^h], w_{R,k-1+\frac{j-1}{q}}) + \int_{t_{k-1}}^{t_k} (\nabla \cdot \boldsymbol{u}_R^h, w_R)\,\mathrm{d}t$$
$$= \int_{t_{k-1}}^{t_k} (f_R, w_R)\,\mathrm{d}t + \int_{t_{k-1}}^{t_k} (g_R(p_R^h), w_R)\,\mathrm{d}t,$$

$$\int_{t_{k-1}}^{t_k} \langle \boldsymbol{n} \cdot (\boldsymbol{u}_L^h - \boldsymbol{u}_R^h), \nu \rangle_{\Gamma_I}\,\mathrm{d}t = 0 \tag{2.7}$$

for all $(w_i, \boldsymbol{v}_i, \nu) \in (W_i^h, \boldsymbol{V}_i^h, \Lambda^h)$, $i = L, R$, and the initial condition $p_0^- = p_0$ specified.

We choose bases for the finite element spaces and obtain a nonlinear matrix-vector equation for the corresponding coefficients of the approximate solution. Abusing notation to denote

the vector of coefficients with respect to the space bases by the same variable name (e.g., $p_L^{h,k}$ denotes the vector of coefficients), the matrix-vector system can be written in block form. For example, in a discretization with two fine time steps for each coarse time step, we obtain (2.8)

$$\left[\begin{array}{cc|cc|cc|c} M_L & -B_L & 0 & 0 & 0 & 0 & C_L \\ B_L^T & Z_L & 0 & 0 & 0 & 0 & 0 \\ \hline 0 & 0 & M_R & -B_R & 0 & 0 & C_{R_1} \\ 0 & 0 & B_R^T & Z_R & 0 & 0 & 0 \\ \hline 0 & 0 & 0 & 0 & M_R & -B_R & C_{R_2} \\ 0 & 0 & 0 & -Z_R & B_R^T & Z_R & 0 \\ \hline C_L^T & 0 & C_{R_1}^T & 0 & C_{R_2}^T & 0 & 0 \end{array}\right] \left[\begin{array}{c} \boldsymbol{u}_L^{h,k+1} \\ p_L^{h,k+1} \\ \hline \boldsymbol{u}_R^{h,k+\frac{1}{2}} \\ p_R^{h,k+\frac{1}{2}} \\ \hline \boldsymbol{u}_R^{h,k+1} \\ p_R^{h,k+1} \\ \hline \xi^{h,k+1} \end{array}\right] = \left[\begin{array}{c} D_L^{k+1} \\ \hline F_L^{k+1} + G_L(p_L^{h,k+1}) + Z_L p_L^{h,k} \\ \hline D_R^{k+\frac{1}{2}} \\ \hline F_R^{k+\frac{1}{2}} + G_R(p_R^{h,k+\frac{1}{2}}) + Z_R p_R^{h,k} \\ \hline D_R^{k+1} \\ \hline F_R^{k+1} + G_R(p_R^{h,k+1}) \\ \hline 0 \end{array}\right].$$

Each matrix block corresponds to one of the inner product terms in the weak form. The jump term corresponds to the blocks Z. Since there are test functions associated with each substep in time on the right, the block that couples the right component to the interface, C_R, appears multiple times.

2.4. Geometrically coupled finite volume discretization. We formulate the finite volume method as a finite element method with special quadrature, as in [18, 2]. We use "geometric coupling" to refer to various schemes for computing coupled quantities derived on heuristic arguments employing only cell values of the approximations. There are many varieties of geometric coupling schemes, and we consider a class that is often encountered in practice. In space, we employ polynomial extrapolation to project state and flux information from one subdomain to the other. In our numerical experiments, we implement both a constant and a linear extrapolation, as in [2]. In time, we consider the scheme in which the approximation values at the end of a composite time step are projected to the other subdomain for use over the entire composite time step. The projection scheme in time is depicted in Figure 3. The projection process in space and time is denoted by the projection operators $P_{R\to L}(p_R^h)$ and $P_{L\to R}(p_L^h)$.

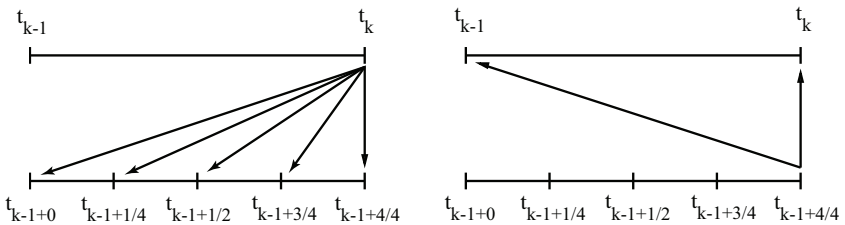

Figure 3. *On the left, the coarse subdomain projects flux values from the end of the composite time step to the fine subdomain. On the right, the fine subdomain projects state values from the end of the composite time step to the coarse subdomain.*

In this paper, we consider the choice of projecting state values from the fine subdomain to the coarse subdomain and flux values from the coarse subdomain to the fine subdomain because this is used on tokamak fusion simulations [10, 11]. It is straightforward to extend the analysis to the reverse choice.

The geometrically coupled finite volume method reads as follows: For $k = 1, 2, \ldots$, compute

$p_i^h \in W_i^h$, $\boldsymbol{u}_i^h \in \boldsymbol{V}_i^h$, $\xi^h \in \Lambda^h$, $i = L, R$, satisfying

$$\int_{t_{k-1}}^{t_k} (a_L^{-1}\boldsymbol{u}_L^h, \boldsymbol{v}_L)_{M,T}\,\mathrm{d}t - \int_{t_{k-1}}^{t_k} (p_L^h, \nabla\cdot\boldsymbol{v}_L)\,\mathrm{d}t + \int_{t_{k-1}}^{t_k} \langle P_{R\to L}(p_R^h), \boldsymbol{n}\cdot\boldsymbol{v}_L\rangle_{\Gamma_I}\,\mathrm{d}t = -\int_{t_{k-1}}^{t_k} \langle d_L, \boldsymbol{n}\cdot\boldsymbol{v}_L\rangle_{\Gamma_L,M}\,\mathrm{d}t,$$

$$\int_{t_{k-1}}^{t_k} (\dot{p}_L^h, w_L)\,\mathrm{d}t + ([p_{L,k-1}^h], w_{L,k-1}) + \int_{t_{k-1}}^{t_k} (\nabla\cdot\boldsymbol{u}_L^h, w_L)\,\mathrm{d}t = \int_{t_{k-1}}^{t_k} (f_L, w_L)\,\mathrm{d}t + \int_{t_{k-1}}^{t_k} (g_L(p_L^h), w_L)\,\mathrm{d}t,$$

$$\int_{t_{k-1}}^{t_k} (a_R^{-1}\boldsymbol{u}_R^h, \boldsymbol{v}_R)_{M,T}\,\mathrm{d}t - \int_{t_{k-1}}^{t_k} (p_R^h, \nabla\cdot\boldsymbol{v}_R)\,\mathrm{d}t - \int_{t_{k-1}}^{t_k} \langle \xi^h, \boldsymbol{n}\cdot\boldsymbol{v}_R\rangle_{\Gamma_I}\,\mathrm{d}t = -\int_{t_{k-1}}^{t_k} \langle d_R, \boldsymbol{n}\cdot\boldsymbol{v}_R\rangle_{\Gamma_R,M}\,\mathrm{d}t,$$

$$\sum_{j=1}^{q} \int_{t_{k-1+\frac{j-1}{q}}^+}^{t_{k-1+\frac{j}{q}}^-} (\dot{p}_R^h, w_R)\,\mathrm{d}t + \sum_{j=1}^{q} ([p_{R,k-1+\frac{j-1}{q}}^h], w_{R,k-1+\frac{j-1}{q}}) + \int_{t_{k-1}}^{t_k} (\nabla\cdot\boldsymbol{u}_R^h, w_R)\,\mathrm{d}t = \int_{t_{k-1}}^{t_k} (f_R, w_R)\,\mathrm{d}t + \int_{t_{k-1}}^{t_k} (g_R(p_R^h), w_R)\,\mathrm{d}t,$$

$$\int_{t_{k-1}}^{t_k} \langle (P_{L\to R}(p_L^h) - \boldsymbol{n}\cdot\boldsymbol{u}_R^h)\,\mathrm{d}t, \nu\rangle_{\Gamma_I}\,\mathrm{d}t = 0 \tag{2.9}$$

for all $(w_i, \boldsymbol{v}_i, \nu) \in (W_i^h, \boldsymbol{V}_i^h, \Lambda^h)$, $i = L, R$, where the approximate inner product is $(\boldsymbol{u}^h, \boldsymbol{v})_{M,T} = (u_x^h, v_x)_{T_x,M_y} + (u_y^h, v_y)_{M_x,T_y}$, where $M_{(\cdot)}$ and $T_{(\cdot)}$ denote the midpoint and trapezoidal quadrature rules in the x- and y-directions as indicated, while $\langle\cdot,\cdot\rangle_{\Gamma_i,M}$ denotes the midpoint rule for $i = L, R$. These choices make the finite element method equivalent to the finite volume method [18, 2, 32, 33].

The resulting discrete nonlinear equations in a discretization with two fine time steps per coarse time step have the block form

(2.10)

$$\left[\begin{array}{cc|cc|cc|c} M_L & -B_L & 0 & Q_{D_1} & 0 & Q_{D_2} & 0 \\ B_L^T & Z_L & 0 & 0 & 0 & 0 & 0 \\ \hline 0 & 0 & M_R & -B_R & 0 & 0 & C_{R_1} \\ 0 & 0 & B_R^T & Z_R & 0 & 0 & 0 \\ \hline 0 & 0 & 0 & 0 & M_R & -B_R & C_{R_2} \\ 0 & 0 & 0 & -Z_R & B_R^T & Z_R & 0 \\ \hline 0 & Q_N & C_{R_1}^T & 0 & C_{R_2}^T & 0 & 0 \end{array}\right] \left[\begin{array}{c} \boldsymbol{u}_L^{h,k+1} \\ \hline p_L^{h,k+1} \\ \hline \boldsymbol{u}_R^{h,k+\frac{1}{2}} \\ \hline p_R^{h,k+\frac{1}{2}} \\ \hline \boldsymbol{u}_R^{h,k+1} \\ \hline p_R^{h,k+1} \\ \hline \xi^{h,k+1} \end{array}\right] = \left[\begin{array}{c} D_L^{k+1} \\ \hline F_L^{k+1} + G_L(p_L^{h,k+1}) + Z_L p_L^{h,k} \\ \hline D_R^{k+\frac{1}{2}} \\ \hline F_R^{k+\frac{1}{2}} + G_R(p_R^{h,k+\frac{1}{2}}) + Z_R p_R^{h,k} \\ \hline D_R^{k+1} \\ \hline F_R^{k+1} + G_R(p_R^{h,k+1}) \\ \hline 0 \end{array}\right].$$

Note that since each substep in time on the right could contribute data in the coupling process, the block Q_D appears multiple times. It is common in practice for only the last substep to contribute, and we follow this practice, as indicated in Figure 3. Therefore in our implementation, Q_{D_1} in (2.10) is zero.

2.5. Iterative solution. The discretizations in sections 2.3 and 2.4 result in large, sparse, nonlinear systems of equations for the coefficients of the approximate solutions. These systems must be solved with an iterative method in general. Solution methods based on a Newton iteration are favored in situations in which it is desirable to avoid the time step restrictions required for methods based on a simple, linearly convergent fixed point iteration. However, there are a number of possible approaches to construct a solution method that employs Newton iteration, and these approaches may have significantly different properties.

A nominal choice is to apply Newton's method directly to the fully coupled systems (2.8) or (2.10). However, in many cases the choice of solution method is based on implementation and/or high performance issues. For example, memory constraints may make it infeasible to implement the nominal approach. Another issue in many cases is the use of different codes to solve the different components. In view of these constraints, we discuss two different iterative approaches that require only single component solves.

Reduction of the discrete systems. To facilitate a decoupling of the solution algorithm into component solves, we first eliminate the variables $\boldsymbol{u}$ and ξ, leaving a system in p only. The variables $\boldsymbol{u}$ and ξ may be recovered from p if desired.

For simplicity, we show the compression of a simplified finite volume system with no substeps within the composite step. Compression of the mortar system, and systems involving substeps, is carried out in the same way. Beginning with

$$\begin{bmatrix} M_L & -B_L & 0 & Q_D & 0 \\ B_L^T & 0 & 0 & 0 & 0 \\ 0 & 0 & M_R & -B_R & C_R \\ 0 & 0 & B_R^T & 0 & 0 \\ 0 & Q_N & C_R^T & 0 & 0 \end{bmatrix} \begin{bmatrix} \boldsymbol{u}_L \\ p_L \\ \boldsymbol{u}_R \\ p_R \\ \xi \end{bmatrix} = \begin{bmatrix} D_L \\ X_L(p_L) \\ D_R \\ X_R(p_R) \\ 0 \end{bmatrix},$$

we eliminate $\boldsymbol{u}$ to get

$$\begin{bmatrix} B_L^T M_L^{-1} B_L & -B_L^T M_L^{-1} Q_D & 0 \\ 0 & B_R^T M_R^{-1} B_R & -B_R^T M_R^{-1} C_R \\ Q_N & C_R^T M_R^{-1} B_R & -C_R^T M_R^{-1} C_R \end{bmatrix} \begin{bmatrix} p_L \\ p_R \\ \xi \end{bmatrix} = \begin{bmatrix} X_L(p_L) - B_L^T M_L^{-1} D_L \\ X_R(p_R) - B_R^T M_R^{-1} D_R \\ -C_R^T M_R^{-1} D_R \end{bmatrix}.$$

Rewriting to simplify the notation, we have

$$\begin{bmatrix} G_L & -Z_D & 0 \\ 0 & G_R & -H_R \\ Z_N & H_R^T & -K_R \end{bmatrix} \begin{bmatrix} p_L \\ p_R \\ \xi \end{bmatrix} = \begin{bmatrix} R_L(p_L) \\ R_R(p_R) \\ S_R \end{bmatrix}.$$

Eliminating ξ gives

$$\begin{bmatrix} G_L & -Z_D \\ -H_R K_R^{-1} Z_N & G_R - H_R K_R^{-1} H_R^T \end{bmatrix} \begin{bmatrix} p_L \\ p_R \end{bmatrix} = \begin{bmatrix} R_L(p_L) \\ R_R(p_R) - H_R K_R^{-1} S_R \end{bmatrix}.$$

Simplifying the notation again, we obtain a system in p with the form

$$\begin{bmatrix} \mathcal{A}_L & \mathcal{C}_L \\ \mathcal{C}_R & \mathcal{A}_R \end{bmatrix} \begin{bmatrix} p_L \\ p_R \end{bmatrix} = \begin{bmatrix} \mathcal{F}_L(p_L) \\ \mathcal{F}_R(p_R) \end{bmatrix}, \tag{2.11}$$

where $\mathcal{C}_L$ and $\mathcal{C}_R$ represent the coupling between the components.

Picard–Newton iteration. A common iterative approach to solving (2.11) is to set up the fixed point iteration

$$\begin{bmatrix} \mathcal{A}_L & 0 \\ 0 & \mathcal{A}_R \end{bmatrix} \begin{bmatrix} p_L^{i+1} \\ p_R^{i+1} \end{bmatrix} = \begin{bmatrix} 0 & -\mathcal{C}_L \\ -\mathcal{C}_R & 0 \end{bmatrix} \begin{bmatrix} p_L^{i} \\ p_R^{i} \end{bmatrix} + \begin{bmatrix} \mathcal{F}_L(p_L) \\ \mathcal{F}_R(p_R) \end{bmatrix}. \tag{2.12}$$

The coupling rules are used to swap data between the subdomains, and the resulting single component systems can be independently solved with Newton's method. This means that the "outer" iteration is a simple, linearly convergent fixed point iteration and the "inner" iteration is Newton's method on the components. We refer to this iteration as the Picard–Newton iteration.

An advantage of this approach is that it is easy to implement and requires minimal communication between the components. Assuming the outer fixed point iteration is convergent, this method produces the implicitly coupled solution in the limit of iteration. In practice, the outer iteration is often performed for a relatively small number of iterations. In that case, iterating the inner Newton method to convergence does not produce the implicitly coupled approximate solution. For example, during the first step of the outer fixed point iteration, Newton's method is being used to solve component problems with outdated interface data, so converging Newton's method means only that component problems with incorrect interface data are solved exactly. A consequence is that incomplete iteration introduces error into the approximate solution that is carried into the next time step.

Newton–Picard iteration. The second approach employs Newton's method directly on (2.11) but applies a simple fixed point iteration to solve the linear system that arises at each step of Newton's method. The linear system to be solved at each step of Newton's method has the form

$$\begin{bmatrix} \mathcal{J}_L & \mathcal{C}_L \\ \mathcal{C}_R & \mathcal{J}_R \end{bmatrix} \begin{bmatrix} \delta_L \\ \delta_R \end{bmatrix} = \begin{bmatrix} \mathcal{A}_L p_L + \mathcal{C}_L p_R - \mathcal{F}_L(p_L) \\ \mathcal{A}_R p_R + \mathcal{C}_R p_L - \mathcal{F}_R(p_R) \end{bmatrix}. \tag{2.13}$$

The simple fixed point iteration has the form

$$\begin{bmatrix} \mathcal{J}_L & 0 \\ 0 & \mathcal{J}_R \end{bmatrix} \begin{bmatrix} \delta_L^{j} \\ \delta_R^{j} \end{bmatrix} = \begin{bmatrix} \mathcal{A}_L p_L + \mathcal{C}_L p_R - \mathcal{F}_L(p_L) \\ \mathcal{A}_R p_R + \mathcal{C}_R p_L - \mathcal{F}_R(p_R) \end{bmatrix} - \begin{bmatrix} 0 & \mathcal{C}_L \\ \mathcal{C}_R & 0 \end{bmatrix} \begin{bmatrix} \delta_L^{j-1} \\ \delta_R^{j-1} \end{bmatrix}. \tag{2.14}$$

We call this the Newton–Picard iteration. In this approach, the outer iteration is Newton's method while the inner iteration is a simple fixed point iteration. The advantage of this approach is that the faster convergence of Newton's method could lead to fewer iterations of the entire system. However, since information is exchanged between the components at each inner iteration, the Picard–Newton iteration requires more frequent communication than the Newton–Picard iteration. Moreover, if relatively few inner fixed point iterations are performed, then the linear equations for Newton's method are not being solved very accurately, which decreases the rate of convergence of the outer Newton iteration.

General comments. Many commonly encountered coupling schemes can be reduced/reformulated to be either a Picard–Newton or a Newton–Picard approach with minor modification. The a posteriori analysis carried out below can be extended to such variations with minor changes. The general approach to the analysis can also be extended to other coupling schemes.

3. A posteriori error analysis. We next derive accurate a posteriori error estimates for a specified quantity of interest determined as a linear functional. With errors $e_{p_i} = p_i - p_i^h$, $e_{\boldsymbol{u}_i} = \boldsymbol{u}_i - \boldsymbol{u}_i^h$, and $e_\xi = \xi - \xi^h$, for $i = L, R$, the error to be estimated is

$$\mathcal{E} = \int_0^T (\boldsymbol{e}_{\boldsymbol{u}_L}, \boldsymbol{\psi}_{\boldsymbol{u}_L})\,\mathrm{d}t + \int_0^T (e_{p_L}, \psi_{p_L})\,\mathrm{d}t + \int_0^T (\boldsymbol{e}_{\boldsymbol{u}_R}, \boldsymbol{\psi}_{\boldsymbol{u}_R})\,\mathrm{d}t + \int_0^T (e_{p_R}, \psi_{p_R})\,\mathrm{d}t + \int_0^T \langle e_\xi, \psi_\xi\rangle_{\Gamma_I}\,\mathrm{d}t + (e_{p_L}(T), \psi_{T_L}) + (e_{p_R}(T), \psi_{T_R}) \tag{3.1}$$

for a specified $\psi = (\boldsymbol{\psi}_{\boldsymbol{u}_L}, \psi_{p_L}, \boldsymbol{\psi}_{\boldsymbol{u}_R}, \psi_{p_R}, \psi_\xi, \psi_{T_L}, \psi_{T_R})$ determining the quantity of interest, such as a weighted average over the domain, the value in a localized region of the domain, or an approximate normal flux across a curve.

To define an adjoint problem, we employ the standard linearization obtained from the integral form of Taylor's theorem,

$$\widehat{g'(p, p^h)} = \int_0^1 g'(sp + (1-s)p^h)\,\mathrm{d}s,$$

so $\widehat{g'(p,p^h)}e_p = g(p) - g(p^h)$. Since a is symmetric, the adjoint problem reads as

$$\begin{cases} a_L^{-1}\boldsymbol{\phi}_L - \nabla\zeta_L = \boldsymbol{\psi}_{\boldsymbol{u}_L}, & (x,y) \in \Omega_L, t \in [0,T), \\ -\dot{\zeta}_L - \nabla\cdot\boldsymbol{\phi}_L - \widehat{g_L'(p_L, p_L^h)}\zeta_L = \psi_{p_L}, & (x,y) \in \Omega_L, t \in [0,T), \\ \zeta_L = 0, & (x,y) \in \Gamma_L, t \in (0,T], \\ \zeta_L = \psi_{T_L}, & (x,y) \in \Omega_L, t = T, \end{cases} \tag{3.2}$$

$$\begin{cases} a_R^{-1}\boldsymbol{\phi}_R - \nabla\zeta_R = \boldsymbol{\psi}_{\boldsymbol{u}_R}, & (x,y) \in \Omega_R, t \in [0,T), \\ -\dot{\zeta}_R - \nabla\cdot\boldsymbol{\phi}_R - \widehat{g_R'(p_R, p_R^h)}\zeta_R = \psi_{p_R}, & (x,y) \in \Omega_R, t \in [0,T), \\ \zeta_R = 0, & (x,y) \in \Gamma_R, t \in (0,T], \\ \zeta_R = \psi_{T_R}, & (x,y) \in \Omega_R, t = T, \end{cases} \tag{3.3}$$

$$\begin{cases} \beta \equiv \zeta_L = \zeta_R, & (x,y) \in \Gamma_I, t \in [0,T), \\ \boldsymbol{n}\cdot(\boldsymbol{\phi}_L - \boldsymbol{\phi}_R) = \psi_\xi, & (x,y) \in \Gamma_I, t \in [0,T). \end{cases} \tag{3.4}$$

There are a number of residuals that are employed in the estimate. We first define some residuals common to all discretizations,

$$\begin{aligned} \boldsymbol{R}_{\boldsymbol{u}_L} &= -a_L^{-1}\boldsymbol{u}_L^h - \nabla p_L^h, \qquad \boldsymbol{R}_{\boldsymbol{u}_R} = -a_R^{-1}\boldsymbol{u}_R^h - \nabla p_R^h, \qquad R_\xi = \boldsymbol{n}\cdot(\boldsymbol{u}_L^h - \boldsymbol{u}_R^h), \\ R_{p_L} &= f_L + g_L(p_L^h) - \nabla\cdot\boldsymbol{u}_L^h - \dot{p}_L^h, \qquad R_{p_R} = f_R + g_R(p_R^h) - \nabla\cdot\boldsymbol{u}_R^h - \dot{p}_R^h. \end{aligned} \tag{3.5}$$

For the geometric coupling method, we use the additional residuals,

$$R_{\mathrm{proj}\ p} = P_{R\to L}(p_R^h) - \xi^h, \qquad R_{\mathrm{proj}\ \boldsymbol{u}} = \boldsymbol{n}\cdot\boldsymbol{u}_L^h - P_{L\to R}(p_L^h). \tag{3.6}$$

We introduce projection operators that map into the finite element space of the discrete forward solution, i.e.,

$$P_L^h : L^2(L^2(\Omega_L);(0,T]) \to W_L^h, \quad P_R^h : L^2(L^2(\Omega_R);(0,T]) \to W_R^h,$$
$$\Pi_L^h : L^2\big((L^2(\Omega_L))^2;(0,T]\big) \to \boldsymbol{V}_L^h, \quad \Pi_R^h : L^2\big((L^2(\Omega_R))^2;(0,T]\big) \to \boldsymbol{V}_R^h,$$
$$Z^h : L^2(L^2(\Gamma_I);(0,T]) \to \Lambda^h.$$

We assume these projections are bounded in L^2 but are otherwise unspecified. In practice, we employ a combination of restriction and averaging to define these projections. Finally, we define the quadrature residuals

$$\begin{aligned}
QE_{\boldsymbol{u}_L}(\Pi_L^h\boldsymbol{\phi}_L) &= \int_0^T (\boldsymbol{R}_{\boldsymbol{u}_L}, \Pi_L^h\boldsymbol{\phi}_L)\,\mathrm{d}t - \int_0^T (\boldsymbol{R}_{\boldsymbol{u}_L}, \Pi_L^h\boldsymbol{\phi}_L)_Q\,\mathrm{d}t,\\
QE_{p_L}(P_L^h\zeta_L) &= \int_0^T (R_{p_L}, P_L^h\zeta_L)\,\mathrm{d}t - \int_0^T (R_{p_L}, P_L^h\zeta_L)_Q\,\mathrm{d}t,\\
QE_{\boldsymbol{u}_R}(\Pi_R^h\boldsymbol{\phi}_R) &= \int_0^T (\boldsymbol{R}_{\boldsymbol{u}_R}, \Pi_R^h\boldsymbol{\phi}_R)\,\mathrm{d}t - \int_0^T (\boldsymbol{R}_{\boldsymbol{u}_R}, \Pi_R^h\boldsymbol{\phi}_R)_Q\,\mathrm{d}t,\\
QE_{p_R}(P_R^h\zeta_R) &= \int_0^T (R_{p_R}, P_R^h\zeta_R)\,\mathrm{d}t - \int_0^T (R_{p_R}, P_R^h\zeta_R)_Q\,\mathrm{d}t,\\
QE_{\xi}(Z^h\beta) &= \int_0^T \langle R_\xi, Z_h\beta\rangle_{\Gamma_I}\,\mathrm{d}t - \int_0^T \langle R_\xi, Z_h\beta\rangle_{\Gamma_{I_Q}}\,\mathrm{d}t,
\end{aligned} \tag{3.7}$$

where the subscript Q indicates the use of the particular quadrature in question. For the geometric coupling method, we employ the terms $QE_{p_L}(P_L^h\zeta_L)$, $QE_{\boldsymbol{u}_R}(\Pi_R^h\boldsymbol{\phi}_R)$, and $QE_{p_R}(P_R^h\zeta_R)$ given above, along with two alternative quadrature residuals,

$$\begin{aligned}
\mathcal{QE}_{\boldsymbol{u}_L}(\Pi_L^h\boldsymbol{\phi}_L) &= \int_0^T (\boldsymbol{R}_{\boldsymbol{u}_L}, \Pi_L^h\boldsymbol{\phi}_L)\,\mathrm{d}t - \int_0^T (\boldsymbol{R}_{\boldsymbol{u}_L}, \Pi_L^h\boldsymbol{\phi}_L)_Q\,\mathrm{d}t\\
&\quad + \int_0^T \langle R_{\text{proj } p}, \boldsymbol{n}\cdot\Pi_L^h\boldsymbol{\phi}_L\rangle_{\Gamma_{I_Q}}\,\mathrm{d}t - \int_0^T \langle R_{\text{proj } p}, \boldsymbol{n}\cdot\Pi_L^h\boldsymbol{\phi}_L\rangle_{\Gamma_I}\,\mathrm{d}t,\\
\mathcal{QE}_{\xi}(Z^h\beta) &= \int_0^T \langle R_\xi, Z_h\beta\rangle_{\Gamma_I}\,\mathrm{d}t - \int_0^T \langle R_\xi, Z_h\beta\rangle_{\Gamma_{I_Q}}\,\mathrm{d}t\\
&\quad + \int_0^T \langle R_{\text{proj } \boldsymbol{u}}, Z^h\beta\rangle_{\Gamma_{I_Q}}\,\mathrm{d}t - \int_0^T \langle R_{\text{proj } \boldsymbol{u}}, Z^h\beta\rangle_{\Gamma_I}\,\mathrm{d}t.
\end{aligned} \tag{3.8}$$

Note that these two quadrature error expressions contain the same terms present in their counterparts in (3.7), as well as an additional term involving the projection residual.

3.1. Estimates for approximations computed without iteration error. We state the theorems in this section and supply proofs in section 5.

Theorem 3.1 (the mortar mixed finite element method). *The error in the quantity of interest defined by* (3.1) *for the approximation* (2.7) *with quadrature satisfies*

$$\begin{aligned}(3.9)\quad \mathcal{E} = &\int_0^T (\boldsymbol{R}_{\boldsymbol{u}_L}, \boldsymbol{\phi}_L - \Pi_L^h \boldsymbol{\phi}_L)\,\mathrm{d}t + \int_0^T (R_{p_L}, \zeta_L - P_L^h \zeta_L)\,\mathrm{d}t + \int_0^T (\boldsymbol{R}_{\boldsymbol{u}_R}, \boldsymbol{\phi}_R - \Pi_R^h \boldsymbol{\phi}_R)\,\mathrm{d}t \\ &+ \int_0^T (R_{p_R}, \zeta_R - P_R^h \zeta_R)\,\mathrm{d}t + \int_0^T \langle R_\xi, \beta - Z_h\beta\rangle_{\Gamma_I}\,\mathrm{d}t + QE_{\boldsymbol{u}_L}(\Pi_L^h \boldsymbol{\phi}_L) \\ &+ QE_{p_L}(P_L^h \zeta_L) + QE_{\boldsymbol{u}_R}(\Pi_R^h \boldsymbol{\phi}_R) + QE_{p_R}(P_R^h \zeta_R) + QE_\xi(Z^h\beta).\end{aligned}$$

Theorem 3.2 (the geometric coupled finite volume method). *The error in the quantity of interest defined by* (3.1) *for the approximation* (2.9) *with quadrature satisfies*

$$\begin{aligned}(3.10)\quad \mathcal{E} = &\int_0^T (\boldsymbol{R}_{\boldsymbol{u}_L}, \boldsymbol{\phi}_L - \Pi_L^h \boldsymbol{\phi}_L)\,\mathrm{d}t + \int_0^T \langle R_{proj\ p}, \boldsymbol{n}\cdot\Pi_L^h \boldsymbol{\phi}_L\rangle_{\Gamma_I}\,\mathrm{d}t + \int_0^T (R_{p_L}, \zeta_L - P_L^h \zeta_L)\,\mathrm{d}t \\ &+ \int_0^T (\boldsymbol{R}_{\boldsymbol{u}_R}, \boldsymbol{\phi}_R - \Pi_R^h \boldsymbol{\phi}_R)\,\mathrm{d}t + \int_0^T (R_{p_R}, \zeta_R - P_R^h \zeta_R)\,\mathrm{d}t \\ &+ \int_0^T \langle R_\xi, \beta - Z_h\beta\rangle_{\Gamma_I}\,\mathrm{d}t + \int_0^T \langle R_{proj\ \boldsymbol{u}}, Z^h\beta\rangle_{\Gamma_I}\,\mathrm{d}t + \mathcal{QE}_{\boldsymbol{u}_L}(\Pi_L^h \boldsymbol{\phi}_L) \\ &+ QE_{p_L}(P_L^h \zeta_L) + QE_{\boldsymbol{u}_R}(\Pi_R^h \boldsymbol{\phi}_R) + QE_{p_R}(P_R^h \zeta_R) + \mathcal{QE}_\xi(Z^h\beta).\end{aligned}$$

Note that (3.10) includes two additional terms involving projection residuals and two additional terms involving quadrature residuals.

3.2. Estimates for approximations computed with iteration error. The estimates (3.9) and (3.10) apply to the approximate solutions obtained by exact solution of the discrete equations. If the approximation is computed using an iterative method with a finite number of iterations, then the estimates must be modified.

There are a number of ways to extend a posteriori error analysis to deal with effects arising from finite iteration; see [14]. Reliably accurate estimates can be obtained if it is possible to numerically solve additional auxiliary adjoint problems that are used to quantify the effects of finite iteration on stability. However, such estimates are computationally expensive to produce. In this paper, we propose an alternative approach to computing a posteriori estimates that involves relatively less computational overhead.

The proposed approach considers the approximation obtained by exact solution of the discrete equations to be a perturbation of the approximation computed with finite iterations, and the latter is used to form the adjoint problem through linearization. We calculate the effect of the "perturbation" on the computed a posteriori error estimate. If R is a residual in the error estimate, we use R^{ex} to denote the residual computed by exactly solving the discrete equations and R to denote the residual expression obtained by finite iteration. We then define the differences for residuals R and quadrature residuals QE as

$$(3.11)\qquad \Delta R = R - R^{ex}, \qquad \Delta QE(f) = \int_0^T (\Delta R, f)_Q\,\mathrm{d}t - \int_0^T (\Delta R, f)\,\mathrm{d}t.$$

Finally, we denote the right-hand side of (3.9) by $\mathcal{T}^{ex}$ and the right-hand side of (3.10) by $\mathcal{V}^{ex}$.

The following theorems present the error estimates for the mortar mixed finite element method and finite volume method with geometric coupling, respectively.

Theorem 3.3 (errors in the mortar mixed finite element method with iteration). *The error estimate for the mortar mixed finite element method with iteration is*

$$\begin{aligned}\mathcal{E} = \mathcal{T}^{ex} &+ \int_0^T (\Delta \boldsymbol{R}_{\boldsymbol{u}_L}, \Pi_L^h \boldsymbol{\phi}_L)\,\mathrm{d}t + \int_0^T (\Delta R_{p_L}, P_L^h \zeta_L)\,\mathrm{d}t + \int_0^T (\Delta \boldsymbol{R}_{\boldsymbol{u}_R}, \Pi_R^h \boldsymbol{\phi}_R)\,\mathrm{d}t \\ &+ \int_0^T (\Delta R_{p_R}, P_R^h \zeta_R)\,\mathrm{d}t + \int_0^T \langle \Delta R_\xi, Z_h \beta\rangle_{\Gamma_I}\,\mathrm{d}t + \Delta QE_{\boldsymbol{u}_L}(\Pi_L^h \boldsymbol{\phi}_L) \\ &+ \Delta QE_{p_L}(P_L^h \zeta_L) + \Delta QE_{\boldsymbol{u}_R}(\Pi_R^h \boldsymbol{\phi}_R) + \Delta QE_{p_R}(P_R^h \zeta_R) + \Delta QE_\xi(Z^h \beta).\end{aligned} \tag{3.12}$$

Theorem 3.4 (errors in the geometric finite volume method with iteration). *The error estimate for the geometrically coupled finite volume method with iteration* (2.9) *including iteration is*

$$\begin{aligned}\mathcal{E} = \mathcal{V}^{ex} &+ \int_0^T (\Delta \boldsymbol{R}_{\boldsymbol{u}_L}, \Pi_L^h \boldsymbol{\phi}_L)\,\mathrm{d}t + \int_0^T \langle \Delta R_{proj\ p}, \boldsymbol{n} \cdot \Pi_L^h \boldsymbol{\phi}_L\rangle_{\Gamma_I}\,\mathrm{d}t + \int_0^T (\Delta R_{p_L}, P_L^h \zeta_L)\,\mathrm{d}t \\ &+ \int_0^T (\Delta \boldsymbol{R}_{\boldsymbol{u}_R}, \Pi_R^h \boldsymbol{\phi}_R)\,\mathrm{d}t + \int_0^T (\Delta R_{p_R}, P_R^h \zeta_R)\,\mathrm{d}t + \int_0^T \langle \Delta R_\xi, Z_h \beta\rangle_{\Gamma_I}\,\mathrm{d}t \\ &+ \int_0^T \langle \Delta R_{proj\ \boldsymbol{u}}, Z^h \beta\rangle_{\Gamma_I}\,\mathrm{d}t + \Delta \mathcal{QE}_{\boldsymbol{u}_L}(\Pi_L^h \boldsymbol{\phi}_L) + \Delta QE_{p_L}(P_L^h \zeta_L) \\ &+ \Delta QE_{\boldsymbol{u}_R}(\Pi_R^h \boldsymbol{\phi}_R) + \Delta QE_{p_R}(P_R^h \zeta_R) + \Delta \mathcal{QE}_\xi(Z^h \beta).\end{aligned} \tag{3.13}$$

3.3. Implementation of the a posteriori estimates. Implementing the a posteriori results in order to obtain computational error estimates requires a number of approximations; see [15]. We briefly describe the main issues peculiar to the results in this paper.

Linearization error. The adjoint problem (3.2)–(3.4) depends on the exact continuous solution p in the linearization term $\widehat{g'(p, p^h)}$. The standard approach replaces this expression by $\widehat{g'(p, p^h)} \approx \widehat{g'(p^h, p^h)} = g'(p^h)$, which works well in usual situations. However, we find that this does not work well when dealing with finite volume discretizations (piecewise constant finite element approximations). Our conjecture is that the low order of accuracy of the approximation affects the accuracy of the Taylor expansion that justifies the standard approach regardless of the accuracy of the approximation value.

In the case of the $RT0$ space, it is possible to postprocess the state and flux solution to obtain a modified state solution that has improved convergence properties; see [2]. We call this solution $\hat{p}^h$, and we implement the adjoint problem using the term $\widehat{g'(\hat{p}^h, p^h)}$. The postprocessing on a grid cell gives $\hat{p}^h = A(x - x_c) + B(y - y_c) + C$, as illustrated in Figure 4, where

$$A = \frac{u_{x_i} + u_{x_{i+1}}}{2a_c}, \qquad B = \frac{u_{y_i} + u_{y_{i+1}}}{2a_c}, \qquad C = p_i, \tag{3.14}$$

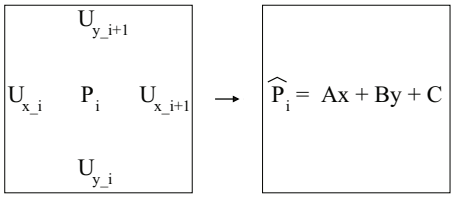

Figure 4. *Postprocessing the p and $\boldsymbol{u}$ values of the RT0 solution into a linear state solution $\hat{p}$.*

and where x_c and y_c are the coordinates of a cell center and a_c is the value of the diffusivity at the cell center. The values A, B, and C represent the first derivatives on the cell and its average value.

In section 4, where we present numerical results, we compare results of using $g'(\widehat{p^h, p^h})$ and $g'(\widehat{\hat{p}^h, p^h})$ in the adjoint problem in Tables 1 and 2.

Solving the adjoint problem. We numerically solve the adjoint problem to obtain numerical approximations $\boldsymbol{\phi}_L \approx \boldsymbol{\phi}_L^h$, $\zeta_L \approx \zeta_L^h$, $\boldsymbol{\phi}_R \approx \boldsymbol{\phi}_R^h$, $\zeta_R \approx \zeta_R^h$, and $\beta \approx \beta^h$. These approximations are used to evaluate the a posteriori error estimates. Computing reliably accurate estimates requires accurately evaluating Galerkin orthogonality [15]. Two possibilities are employing an approximation scheme that is higher order in both space and time than that used for the forward problem, even on a coarser mesh, or to compute an approximation using the same scheme as used for the forward problem but solved on a finer mesh.

For finite volume codes, it is generally problematic to implement higher order approximations. For this reason, we solve the adjoint problem using the same method as the forward problem but on a refined mesh. In the numerical experiments below, we explore the effects of varying the degree of refinement on the accuracy of the estimate.

Evaluating the effects of finite iteration. Evaluating the effects of finite iteration on the residuals, e.g., ΔR, nominally involves computing the residuals for the approximation obtained by exact solution of the discrete equation. For the sake of exploring the effects from finite iteration accurately, we obtain a reference approximation by inverting the system associated with each composite time step directly. In practice, a reference approximation is obtained by solving the discrete equations using additional iterations.

4. Numerical experiments.

In this section, we present a number of numerical experiments. The computations in section 4.2 illustrate the accuracy of the estimate while varying various computational aspects. The computations in section 4.3 explore the performance differences between the mortar and geometric-coupled approximations. In the latter case, we focus on time behavior since [2] contains a thorough investigation of the accuracy issues in space. We also investigate the effect of using a finite number of iterations in the iterative solution of the approximations.

4.1. Computational details.

We set $\Omega_L = [-1, 1] \times [-2, 0]$ and $\Omega_R = [-1, 1] \times [0, 2]$. The interface Γ_I is located along $y = 0$. The final time T is specified for each experiment.

The grids are reported as $n_L \times m_L \times k_L$ for the left domain and $n_R \times m_R \times k_R$ for the right domain, where $n_{(\cdot)}$ corresponds to the number of cells in the x-direction (which is also the

number of cells along the interface), $m_{(\cdot)}$ corresponds to the number of cells in the y-direction, and $k_{(\cdot)}$ corresponds to the number of time steps.

In order to compare the relative sizes of various contributions to the error, we report values for the terms in the error estimates given in Theorems 3.1 and 3.2. Recalling (3.5) and (3.6), the following terms are included for both the mixed finite element and geometric finite volume methods:

$$T_1 = (\boldsymbol{R}_{\boldsymbol{u}_L}, \boldsymbol{\phi}_L^h - \Pi_L^h \boldsymbol{\phi}_L^h), \qquad T_2 = (\boldsymbol{R}_{\boldsymbol{u}_R}, \boldsymbol{\phi}_R^h - \Pi_R^h \boldsymbol{\phi}_R^h), \qquad T_3 = (R_{p_L}, \zeta_L^h - P_L^h \zeta_L^h),$$
$$T_4 = (R_{p_R}, \zeta_R^h - P_R^h \zeta_R^h), \qquad T_5 = \langle R_\xi, \beta^h - Z_h \beta^h \rangle_{\Gamma_I}.$$

In the geometric finite volume case, we add

$$T_6 = \langle R_{\text{proj } p}, \boldsymbol{n} \cdot \Pi_L^h \boldsymbol{\phi}_L^h \rangle_{\Gamma_I}, T_7 = \langle R_{\text{proj } \boldsymbol{u}}, Z^h \beta^h \rangle_{\Gamma_I}, T_8 = \mathcal{QE}_{\boldsymbol{u}_L}(\Pi_L^h \boldsymbol{\phi}_L^h), T_9 = QE_{\boldsymbol{u}_R}(\Pi_R^h \boldsymbol{\phi}_R^h).$$

The effect of quadrature on the accuracy of the finite element approximation is investigated in [18, 2]. Hence, we implement the mortar finite element method using a Gaussian quadrature of sufficient order to exactly integrate all polynomial integrands in the weak form encountered in the examples. For nonpolynomial integrands, we use eighth order Gaussian quadrature in each direction, which reduces the quadrature residual terms in Theorem 3.1 to machine precision. Therefore, we evaluate only the terms T_1 through T_5 in the error estimate.

In the case of the geometric finite volume method, we have, in addition to T_1 through T_5, two projection related residual terms and two nonzero quadrature residual terms. Employing the same high order Gaussian quadrature rule leads to three of the five quadrature residual terms in Theorem 3.2 being of machine precision. Moreover, $\mathcal{QE}_{\boldsymbol{u}_L}(\Pi_L^h \boldsymbol{\phi}_L^h)$ in (3.8) involves geometric projection and we use quadrature rules sufficient to integrate the projection terms in the weak form to machine precision. Consequently, the projection-related portion of $\mathcal{QE}_{\boldsymbol{u}_L}(\Pi_L^h \boldsymbol{\phi}_L^h)$ is zero. However, the quadrature residual terms associated with the midpoint and trapezoid rules used to generate the finite volume discretization are significant and are included in the evaluation of the estimate.

In the tables of results below, we use the labels

$$\text{exact } = \sum (e, \psi), \qquad \text{estimate } = \sum T_i.$$

Note that "exact" represents the computation of terms of the form (e, ψ) directly, which requires that the continuous solution of the problem be known in advance. We use the method of manufactured solutions to produce problems with known solutions. The "estimate" involves the approximation of the terms T_i using a numerical solution of the modified adjoint equation. Differences between "exact" and "estimate" arise from change of linearization point for the adjoint problem and the numerical solution. The exact to estimate ratio provides a convenient way to quantify the accuracy of the estimate.

As a gross measure of the effect of geometric projection and of the use of finite volume quadrature, we report the following two ratios in the case of the geometric method:

$$\text{ratio}_{\text{proj}} = \sum_{i=6}^{7} | T_i | \Big/ \sum_{i=1}^{5} | T_i |, \qquad \text{ratio}_{\text{quad}} = \sum_{i=8}^{9} | T_i | \Big/ \sum_{i=1}^{5} | T_i | . \tag{4.1}$$

4.2. Investigation of the accuracy of the estimate. We begin with a problem designed to illustrate the accuracy of the error estimates. We set $a \equiv 1$, $g(p) = p - p^3$, and $T = 2$. Using the method of manufactured solutions, we define the solution to be

$$p(x, y, t) = \cos\left(\frac{\pi x}{2}\right) \cos\left(\frac{\pi y}{4}\right) \times te^{-t} \tag{4.2}$$

and compute the forcing f, the boundary data d, and the initial data p_0 from (4.2) to match. Since the true solution is known, we can compute the exact error. The numerical solution is obtained by using sufficient Newton iterations at each time step to ensure the residual is on the order of machine precision.

In order to investigate issues of accuracy relating to the quality of the numerical adjoint solution, we also use a manufactured solution to the adjoint problem. We define the adjoint solution to be

$$\zeta(x, y, t) = \cos\left(\frac{\pi x}{2}\right) \cos\left(\frac{\pi y}{4}\right) \times te^{-t} \tag{4.3}$$

and compute the adjoint data to yield this solution.

4.2.1. Effect of linearization in the adjoint problem. To test the effect of various approximations to the linearized term in the adjoint problem, we compare results obtained using $\widehat{g'(p, p^h)}$ exactly with $\widehat{g'(p^h, p^h)}$ and $\widehat{g'(\hat{p}^h, p^h)}$ in Table 1. Each of the three choices for the linearized term produces a different system of "adjoint" equations. The true adjoint involves $\widehat{g'(p, p^h)}$. The two other choices result in perturbations to the true adjoint system. In each case we use the same manufactured solution, given by (4.3). The data, ψ, is then computed according to (3.2)–(3.4).

Table 1

Accuracy results for various implementations of $\widehat{g'(p, p^h)}$. The forward grids are $5 \times 5 \times 5 : 8 \times 8 \times 10$.

Linearization	exact	estimate	Ratio
$\widehat{g'(p, p^h)}$	$1.36E{-}2$	$1.36E{-}2$	1.00
$\widehat{g'(\hat{p}^h, p^h)}$	$1.32E{-}2$	$1.36E{-}2$	1.03
$\widehat{g'(p^h, p^h)}$	$1.28E{-}2$	$1.36E{-}2$	1.06

We next show in Table 2 accuracy results for estimates computed using $\widehat{g'(\hat{p}^h, p^h)}$ on several forward grids.

Table 2

Accuracy results obtained using $\widehat{g'(\hat{p}^h, p^h)}$ in the adjoint problem and various grids for the forward problem.

Grid	exact	estimate	Ratio
$5 \times 5 \times 5 : 8 \times 8 \times 10$	$1.32E{-}2$	$1.36E{-}2$	1.03
$10 \times 10 \times 10 : 16 \times 16 \times 20$	$-7.46E{-}3$	$-7.37E{-}3$	.988
$20 \times 20 \times 20 : 32 \times 32 \times 40$	$-3.22E{-}3$	$-3.21E{-}3$	.997

As illustrated in these results, the effect of the linearization approximation generally appears to decrease as the forward grid is refined. We employ $\widehat{g'(\hat{p}^h, p^h)}$ for the rest of the experiments.

4.2.2. Effect of numerical solution of the adjoint problem. We now illustrate the accuracy of the estimate computed with a numerical adjoint solution. Continuing with the same problem, we set the forward grid to $5 \times 5 \times 5 : 8 \times 8 \times 10$. In Table 3 we present the error estimate when computing the adjoint problem using $g'(\widehat{\hat{p}^h, p^h})$ on a sequence of increasingly fine grids.

Table 3
Accuracy results obtained using various discrete adjoint grids.

Adjoint grid	exact	estimate	Ratio
$10 \times 10 \times 10 : 16 \times 16 \times 20$	$1.32E{-}2$	$8.74E{-}3$	.662
$20 \times 20 \times 20 : 32 \times 32 \times 40$	$1.32E{-}2$	$1.15E{-}2$	.871
$40 \times 40 \times 40 : 64 \times 64 \times 80$	$1.32E{-}2$	$1.27E{-}2$	.961
$80 \times 80 \times 80 : 128 \times 128 \times 160$	$1.32E{-}2$	$1.31E{-}2$	.993

4.2.3. Conclusions. These results show that accuracy of the computed estimation is mildly affected by the various numerical discretization steps required to actually implement the a posteriori error estimate. It is worth nothing that solving the adjoint problem using a mesh with only half the mesh size diameter causes significant error in the resulting estimate, though this is a common choice.

4.3. A problem with significant scale differences in the components. We next consider a problem with significant scale differences in the components motivated by the coupling of core and edge processes in a tokamak fusion reactor [10, 11]. The solution in one component varies only in one spatial dimension while the solution in the other component varies in two spatial dimensions, which presents an extreme case since a single cell spanning the interface in the first component is coupled to many cells in the second component. Moreover, the solution behavior in time is much faster in the component with two dimensional behavior, and we use a substepping ratio of 10 to capture this.

We set $a \equiv 1$ and $g \equiv 0$ and compute the source f that corresponds to the manufactured solution

$$p(x,y) = \cos\left(\frac{\pi(y+2)}{8}\right)e^{-t} + 0.3\,\sin(\pi x)\cos(5(2\pi t))\left[\frac{1-\tanh\big(2(1-y)\big)}{2}\right]. \tag{4.4}$$

This solution, shown in Figure 5, has the desired behavior in space and time. We note that the $\sin(x)$ shaped wave on Ω_R oscillates from a $\sin(x)$ to a $-\sin(x)$ shape 10 times per unit of simulation time while the $\cos(y)$ portion of the solution decays as e^{-t}. We use the same forcing function f in the problem with the nonlinearity $g(p) = p - p^3$. The resulting problem no longer has a manufactured solution, but the solution exhibits the same qualitative behavior.

For adjoint data, we use $\boldsymbol{\psi_p}$ and both components of $\boldsymbol{\psi_u}$ that form "ridges" near $y = 1$, i.e., in the middle of the finer subdomain, along with a constant ψ_ζ at the interface. These functions have the form $Ce^{-(y-1)^2}$ and are plotted in Figure 6.

We present the results for both a short time period $[0, 1]$ and a longer period $[0, 4]$. The grids are forward $1 \times 16 \times 10 : 16 \times 16 \times 100$ and adjoint $32 \times 32 \times 20 : 32 \times 32 \times 200$ for the short simulation, and forward $1 \times 16 \times 40 : 16 \times 16 \times 400$ and adjoint $32 \times 32 \times 80 : 32 \times 32 \times 800$ for the long simulation.

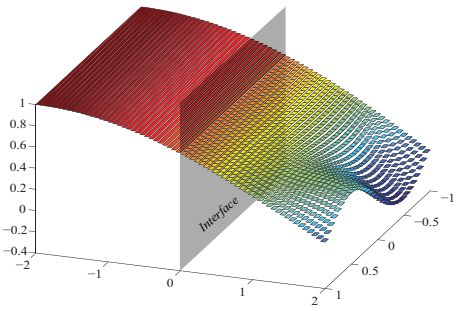

Figure 5. *Plot of the solution* (4.4) *at one time.*

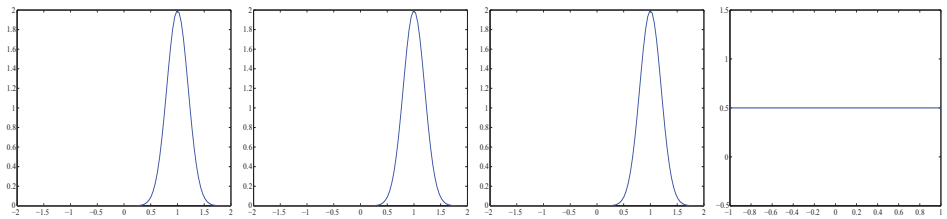

Figure 6. *Adjoint data profiles. The plots of ψ_{u_x}, ψ_{u_y}, and ψ_p are shown in one dimension because they have no variation in the x-direction, and ψ_ξ is a one dimensional function defined on the interface.*

We list contributions to the error estimate for the mortar mixed finite element method and for the geometrically coupled finite volume method using both constant and linear extrapolation to approximate coupling values. In the constant case, the state or flux value nearest the interface in space is used as a boundary condition for the other domain. In the linear case, the two values nearest the interface in space are used to compute a linear extrapolation at the interface. In both cases, the values at the end time of the composite step are used to provide data for the other component, as described in Figure 3.

4.3.1. Results for approximations computed with exact solution of the discrete equations. We first consider results for approximations computed with exact solution of the discrete equations. In all cases, we use five Newton iterations on the entire implicit system on each composite time step, which leads to a Newton residual on the order of machine precision.

The results in Table 4 show that the error estimate for the geometric finite volume method is an order of magnitude larger than it is for the mortar method, with the largest contributions coming from the quadrature and geometric projections. The contributions due to geometric projection are larger for the constant extrapolation than they are for the linear extrapolation, especially the term associated with the projected flux, which is an order of magnitude larger in the constant case. Table 5 shows that these trends continue in the long simulation, with the difference in the error estimate between the mortar and geometric methods rising to two orders of magnitude, and the difference in the size of the term associated with projected flux between the constant and linear geometric methods also rising to two orders of magnitude.

Table 4

Error contributions for the short time period with exact inversion at each Newton step and five Newton steps per composite time step.

Term		MFE	GFV (linear)	GFV (constant)
1	$(\boldsymbol{R}_{\boldsymbol{u}_L}, \boldsymbol{\phi}_L^h - \Pi_L^h \boldsymbol{\phi}_L^h)$	$-4.2E{-3}$	$-3.6E{-3}$	$-3.3E{-3}$
2	$(\boldsymbol{R}_{\boldsymbol{u}_R}, \boldsymbol{\phi}_R^h - \Pi_R^h \boldsymbol{\phi}_R^h)$	$-1.5E{-4}$	$-2.1E{-4}$	$-2.1E{-4}$
3	$(R_{p_L}, \zeta_L^h - P_L^h \zeta_L^h)$	$1.8E{-3}$	$1.4E{-3}$	$1.4E{-3}$
4	$(R_{p_R}, \zeta_R^h - P_R^h \zeta_R^h)$	$3.4E{-4}$	$3.1E{-4}$	$3.2E{-4}$
5	$\langle R_\xi, \beta^h - Z_h \beta^h \rangle_{\Gamma_I}$	$1.6E{-17}$	$9.4E{-6}$	$1.6E{-4}$
6	$\langle R_{\text{proj } p}, \boldsymbol{n} \cdot \Pi_L^h \boldsymbol{\phi}_L^h \rangle_{\Gamma_I}$	N/A	$-9.7E{-3}$	$-2.0E{-2}$
7	$\langle R_{\text{proj } \boldsymbol{u}}, Z^h \beta^h \rangle_{\Gamma_I}$	N/A	$5.7E{-4}$	$9.3E{-3}$
8	$\mathcal{QE}_{\boldsymbol{u}_L}(\Pi_L^h \boldsymbol{\phi}_L^h)$	N/A	$-2.3E{-2}$	$-2.0E{-2}$
9	$QE_{\boldsymbol{u}_R}(\Pi_R^h \boldsymbol{\phi}_R^h)$	N/A	$-8.1E{-4}$	$-7.9E{-4}$
Total		$-2.2E{-3}$	$-3.5E{-2}$	$-3.3E{-2}$
$\text{ratio}_{\text{proj}}$		N/A	1.9	5.3
$\text{ratio}_{\text{quad}}$		N/A	4.3	3.8

Table 5

Error contributions for the long time period with exact inversion at each Newton step and five Newton steps per composite time step.

Term		MFE	GFV (linear)	GFV (constant)
1	$(\boldsymbol{R}_{\boldsymbol{u}_L}, \boldsymbol{\phi}_L^h - \Pi_L^h \boldsymbol{\phi}_L^h)$	$4.2E{-3}$	$-8.1E{-3}$	$-7.4E{-3}$
2	$(\boldsymbol{R}_{\boldsymbol{u}_R}, \boldsymbol{\phi}_R^h - \Pi_R^h \boldsymbol{\phi}_R^h)$	$1.4E{-4}$	$-1.4E{-4}$	$-1.0E{-4}$
3	$(R_{p_L}, \zeta_L^h - P_L^h \zeta_L^h)$	$-8.3E{-4}$	$-4.1E{-4}$	$-4.6E{-4}$
4	$(R_{p_R}, \zeta_R^h - P_R^h \zeta_R^h)$	$2.4E{-6}$	$3.2E{-5}$	$2.9E{-5}$
5	$\langle R_\xi, \beta^h - Z_h \beta^h \rangle_{\Gamma_I}$	$-1.3E{-17}$	$-1.7E{-6}$	$5.3E{-4}$
6	$\langle R_{\text{proj } p}, \boldsymbol{n} \cdot \Pi_L^h \boldsymbol{\phi}_L^h \rangle_{\Gamma_I}$	N/A	$-2.4E{-2}$	$-4.8E{-2}$
7	$\langle R_{\text{proj } \boldsymbol{u}}, Z^h \beta^h \rangle_{\Gamma_I}$	N/A	$-1.3E{-4}$	$3.7E{-2}$
8	$\mathcal{QE}_{\boldsymbol{u}_L}(\Pi_L^h \boldsymbol{\phi}_L^h)$	N/A	$-2.3E{-1}$	$-2.1E{-1}$
9	$QE_{\boldsymbol{u}_R}(\Pi_R^h \boldsymbol{\phi}_R^h)$	N/A	$-4.0E{-3}$	$-3.8E{-3}$
Total		$3.5E{-3}$	$-2.7E{-1}$	$-2.3E{-1}$
$\text{ratio}_{\text{proj}}$		N/A	2.7	9.8
$\text{ratio}_{\text{quad}}$		N/A	26.8	25.0

4.3.2. Results for approximations computed with iterative solution of the discrete equations with a finite number of iterations. Next, we repeat the test while employing the Newton–Picard method described in section 2.5 at each time step to solve the discrete equations for the approximation. Tables 6 through 9 show the results for the short time period. We performed the computation using five Newton steps and either 50, 10, 3, or 1 Picard iterations per Newton step over each composite time step. Using 50 iterations yields results identical to those obtained with exact solution. However, if we use 10 or fewer iterations, we find that Newton's method does not converge to machine precision in five iterations. We present the results for the long period computation employing three iterations per Newton step in Table 10.

In addition to the terms listed in the tables above, the Δ terms associated with the iterative method are also listed. Each table also lists the convergence rate for the inner fixed point iteration. Given that the same number of iterations is used for all methods, any method

with slower convergence clearly has larger Δ terms. It is interesting to note that while linear extrapolation produces better results than constant extrapolation if solved exactly, it results in a slower convergence rate and might therefore perform worse than constant extrapolation when the same number of inner iterations are used.

Table 6

Error contributions for the short time period computation using 50 iterations per Newton step and five Newton steps per composite time step.

Term		MFE	GFV (linear)	GFV (constant)
1	$(\boldsymbol{R}_{\boldsymbol{u}_L}, \boldsymbol{\phi}_L^h - \Pi_L^h \boldsymbol{\phi}_L^h)$	$-4.2E{-3}$	$-3.6E{-3}$	$-3.3E{-3}$
2	$(\boldsymbol{R}_{\boldsymbol{u}_R}, \boldsymbol{\phi}_R^h - \Pi_R^h \boldsymbol{\phi}_R^h)$	$-1.5E{-4}$	$-2.1E{-4}$	$-2.1E{-4}$
3	$(R_{p_L}, \zeta_L^h - P_L^h \zeta_L^h)$	$1.8E{-3}$	$1.4E{-3}$	$1.4E{-3}$
4	$(R_{p_R}, \zeta_R^h - P_R^h \zeta_R^h)$	$3.4E{-4}$	$3.1E{-4}$	$3.2E{-4}$
5	$\langle R_\xi, \beta^h - Z_h \beta^h \rangle_{\Gamma_I}$	$-1.3E{-17}$	$9.4E{-6}$	$1.6E{-4}$
6	$\langle R_{\text{proj } p}, \boldsymbol{n} \cdot \Pi_L^h \boldsymbol{\phi}_L^h \rangle_{\Gamma_I}$	N/A	$-9.7E{-3}$	$-2.0E{-2}$
7	$\langle R_{\text{proj } \boldsymbol{u}}, Z^h \beta^h \rangle_{\Gamma_I}$	N/A	$5.7E{-4}$	$9.3E{-3}$
8	$\mathcal{QE}_{\boldsymbol{u}_L}(\Pi_L^h \boldsymbol{\phi}_L^h)$	N/A	$-2.3E{-2}$	$-2.0E{-2}$
9	$QE_{\boldsymbol{u}_R}(\Pi_R^h \boldsymbol{\phi}_R^h)$	N/A	$-8.1E{-4}$	$-7.9E{-4}$
Res total		$-2.2E{-3}$	$-3.5E{-2}$	$-3.3E{-2}$
1	$(\Delta \boldsymbol{R}_{\boldsymbol{u}_L}, \Pi_L^h \boldsymbol{\phi}_L^h)$	$1.7E{-16}$	$1.7E{-15}$	$1.7E{-17}$
2	$(\Delta \boldsymbol{R}_{\boldsymbol{u}_R}, \Pi_R^h \boldsymbol{\phi}_R^h)$	$3.9E{-16}$	$5.6E{-17}$	$3.1E{-17}$
3	$(\Delta R_{p_L}, P_L^h \zeta_L^h)$	$4.2E{-17}$	$1.4E{-13}$	$2.8E{-17}$
4	$(\Delta R_{p_R}, P_R^h \zeta_R^h)$	$1.1E{-16}$	$-8.4E{-15}$	$-1.4E{-17}$
5	$\langle \Delta R_\xi, Z_h \beta^h \rangle_{\Gamma_I}$	$3.7E{-17}$	$-1.5E{-13}$	$-1.4E{-16}$
6	$\langle \Delta R_{\text{proj } p}, \boldsymbol{n} \cdot \Pi_L^h \boldsymbol{\phi}_L^h \rangle_{\Gamma_I}$	N/A	$-9.3E{-16}$	$-1.7E{-17}$
7	$\langle \Delta R_{\text{proj } \boldsymbol{u}}, Z^h \beta^h \rangle_{\Gamma_I}$	N/A	$1.5E{-13}$	$7.8E{-17}$
8	$\Delta \mathcal{QE}_{\boldsymbol{u}_L}(\Pi_L^h \boldsymbol{\phi}_L^h)$	N/A	$-8.7E{-16}$	$6.9E{-18}$
9	$\Delta QE_{\boldsymbol{u}_R}(\Pi_R^h \boldsymbol{\phi}_R^h)$	N/A	$-1.0E{-17}$	$-1.4E{-17}$
Iterative total		$7.5E{-16}$	$1.3E{-13}$	$-7.6E{-17}$
Overall total		$-2.2E{-3}$	$-3.5E{-2}$	$-3.3E{-2}$
Conv. rate		.74	.89	.71
$\text{ratio}_{\text{proj}}$		N/A	1.9	5.3
$\text{ratio}_{\text{quad}}$		N/A	4.3	3.8

The results indicate that if the number of iterations is sufficiently large that the Δ terms are small relative to the residual terms, then the superiority of the mortar method remains intact. However if the error due to incomplete iteration becomes large compared to the residual error, then both methods suffer and the difference in performance between the two methods disappears.

5. Proofs.

5.1. Proof of Theorem 3.1. The proof begins by substituting the corresponding expressions from the left-hand side of the adjoint problem (3.2)–(3.4) for ψ in (3.1). Integration and applying the divergence theorem yield

$$\mathcal{E} = \int_0^T (\boldsymbol{e}_{\boldsymbol{u}_L}, a^{-1}\boldsymbol{\phi}_L)\,\mathrm{d}t + \int_0^T (\nabla \cdot \boldsymbol{e}_{\boldsymbol{u}_L}, \zeta_L)\,\mathrm{d}t - \int_0^T \langle \boldsymbol{n} \cdot \boldsymbol{e}_{\boldsymbol{u}_L}, \beta \rangle_{\Gamma_I}\,\mathrm{d}t - \int_0^T (e_{p_L}, \nabla \cdot \boldsymbol{\phi}_L)\,\mathrm{d}t$$

Table 7

Error contributions for the short time period test with 10 iterations per Newton step and five Newton steps per composite time step.

Term		MFE	GFV (linear)	GFV (constant)
1	$(\boldsymbol{R}_{\boldsymbol{u}_L}, \boldsymbol{\phi}_L^h - \Pi_L^h \boldsymbol{\phi}_L^h)$	$-4.2E{-}3$	$-3.5E{-}3$	$-3.3E{-}3$
2	$(\boldsymbol{R}_{\boldsymbol{u}_R}, \boldsymbol{\phi}_R^h - \Pi_R^h \boldsymbol{\phi}_R^h)$	$-1.5E{-}4$	$-2.1E{-}4$	$-2.1E{-}4$
3	$(R_{p_L}, \zeta_L^h - P_L^h \zeta_L^h)$	$1.8E{-}3$	$1.4E{-}3$	$1.4E{-}3$
4	$(R_{p_R}, \zeta_R^h - P_R^h \zeta_R^h)$	$3.4E{-}4$	$3.1E{-}4$	$3.2E{-}4$
5	$\langle R_\xi, \beta^h - Z_h \beta^h \rangle_{\Gamma_I}$	$-4.3E{-}19$	$2.3E{-}5$	$1.6E{-}4$
6	$\langle R_{\text{proj } p}, \boldsymbol{n} \cdot \Pi_L^h \boldsymbol{\phi}_L^h \rangle_{\Gamma_I}$	N/A	$-9.7E{-}3$	$-2.0E{-}2$
7	$\langle R_{\text{proj } \boldsymbol{u}}, Z^h \beta^h \rangle_{\Gamma_I}$	N/A	$1.4E{-}3$	$9.3E{-}3$
8	$\mathcal{QE}_{\boldsymbol{u}_L}(\Pi_L^h \boldsymbol{\phi}_L^h)$	N/A	$-2.3E{-}2$	$-2.0E{-}2$
9	$QE_{\boldsymbol{u}_R}(\Pi_R^h \boldsymbol{\phi}_R^h)$	N/A	$-8.0E{-}4$	$-7.9E{-}4$
Res total		$-2.2E{-}3$	$-3.4E{-}2$	$-3.3E{-}2$
1	$(\Delta \boldsymbol{R}_{\boldsymbol{u}_L}, \Pi_L^h \boldsymbol{\phi}_L^h)$	$5.6E{-}17$	$-4.6E{-}6$	$9.3E{-}11$
2	$(\Delta \boldsymbol{R}_{\boldsymbol{u}_R}, \Pi_R^h \boldsymbol{\phi}_R^h)$	$-8.3E{-}17$	$6.9E{-}8$	$6.4E{-}13$
3	$(\Delta R_{p_L}, P_L^h \zeta_L^h)$	$-1.8E{-}8$	$-7.0E{-}4$	$-6.2E{-}9$
4	$(\Delta R_{p_R}, P_R^h \zeta_R^h)$	$-1.9E{-}8$	$1.5E{-}4$	$1.7E{-}9$
5	$\langle \Delta R_\xi, Z_h \beta^h \rangle_{\Gamma_I}$	$2.5E{-}17$	$7.9E{-}4$	$7.0E{-}9$
6	$\langle \Delta R_{\text{proj } p}, \boldsymbol{n} \cdot \Pi_L^h \boldsymbol{\phi}_L^h \rangle_{\Gamma_I}$	N/A	$2.1E{-}5$	$9.1E{-}11$
7	$\langle \Delta R_{\text{proj } \boldsymbol{u}}, Z^h \beta^h \rangle_{\Gamma_I}$	N/A	$-7.9E{-}4$	$-7.0E{-}9$
8	$\Delta \mathcal{QE}_{\boldsymbol{u}_L}(\Pi_L^h \boldsymbol{\phi}_L^h)$	N/A	$-1.6E{-}5$	$-1.8E{-}10$
9	$\Delta QE_{\boldsymbol{u}_R}(\Pi_R^h \boldsymbol{\phi}_R^h)$	N/A	$-6.9E{-}8$	$-6.4E{-}13$
Iterative total		$-3.7E{-}8$	$-5.6E{-}4$	$-4.6E{-}9$
Overall total		$-2.2E{-}3$	$-3.5E{-}2$	$-3.3E{-}2$
Conv. rate		.74	.89	.71
$\text{ratio}_{\text{proj}}$		N/A	2.0	5.3
$\text{ratio}_{\text{quad}}$		N/A	4.3	3.8

$$
\begin{aligned}
&- \int_0^T (e_{p_L}, \dot{\zeta}_L)\,\mathrm{d}t + (e_{p_L}(T), \zeta_L(T)) + \int_0^T (e_{p_L}, -g_L'\widehat{(p_L, p_L^h)}\zeta_L)\,\mathrm{d}t \\
&+ \int_0^T (\boldsymbol{e}_{\boldsymbol{u}_R}, a^{-1}\boldsymbol{\phi}_R)\,\mathrm{d}t + \int_0^T (\nabla \cdot \boldsymbol{e}_{\boldsymbol{u}_R}, \zeta_R)\,\mathrm{d}t + \int_0^T \langle \boldsymbol{n} \cdot \boldsymbol{e}_{\boldsymbol{u}_R}, \beta \rangle_{\Gamma_I}\,\mathrm{d}t - \int_0^T (e_{p_R}, \nabla \cdot \boldsymbol{\phi}_R)\,\mathrm{d}t \\
&- \int_0^T (e_{p_R}, \dot{\zeta}_R)\,\mathrm{d}t + (e_{p_R}(T), \zeta_R(T)) + \int_0^T (e_{p_R}, -g_R'\widehat{(p_R, p_R^h)}\zeta_R)\,\mathrm{d}t \\
&+ \int_0^T \langle e_\xi, \boldsymbol{n} \cdot (\boldsymbol{\phi}_L - \boldsymbol{\phi}_R) \rangle_{\Gamma_I}\,\mathrm{d}t.
\end{aligned}
$$

Since ζ is continuous, integration by parts in time and using $e(0) = 0$ give

$$
\int_0^T (e, \dot{\zeta})\,\mathrm{d}t = (e(T), \zeta(T)) - \int_0^T (\dot{e}, \zeta)\,\mathrm{d}t.
$$

Cancellation yields

$$
\mathcal{E} = \int_0^T (\boldsymbol{e}_{\boldsymbol{u}_L}, a^{-1}\boldsymbol{\phi}_L)\,\mathrm{d}t + \int_0^T (\nabla \cdot \boldsymbol{e}_{\boldsymbol{u}_L}, \zeta_L)\,\mathrm{d}t - \int_0^T \langle \boldsymbol{n} \cdot \boldsymbol{e}_{\boldsymbol{u}_L}, \beta \rangle_{\Gamma_I}\,\mathrm{d}t - \int_0^T (e_{p_L}, \nabla \cdot \boldsymbol{\phi}_L)\,\mathrm{d}t
$$

Table 8

Error contributions for the short time period test with three iterations per Newton step and five Newton steps per composite time step.

Term		MFE	GFV (linear)	GFV (constant)
1	$(\boldsymbol{R}_{\boldsymbol{u}_L}, \boldsymbol{\phi}_L^h - \Pi_L^h \boldsymbol{\phi}_L^h)$	$-4.2E{-3}$	$-3.4E{-3}$	$-3.3E{-3}$
2	$(\boldsymbol{R}_{\boldsymbol{u}_R}, \boldsymbol{\phi}_R^h - \Pi_R^h \boldsymbol{\phi}_R^h)$	$-1.5E{-4}$	$-2.1E{-4}$	$-2.1E{-4}$
3	$(R_{p_L}, \zeta_L^h - P_L^h \zeta_L^h)$	$1.8E{-3}$	$1.4E{-3}$	$1.4E{-3}$
4	$(R_{p_R}, \zeta_R^h - P_R^h \zeta_R^h)$	$3.4E{-4}$	$3.1E{-4}$	$3.2E{-4}$
5	$\langle R_\xi, \beta^h - Z_h \beta^h \rangle_{\Gamma_I}$	$-1.5E{-17}$	$-4.4E{-4}$	$1.4E{-4}$
6	$\langle R_{\text{proj } p}, \boldsymbol{n} \cdot \Pi_L^h \boldsymbol{\phi}_L^h \rangle_{\Gamma_I}$	N/A	$-1.1E{-2}$	$-2.0E{-2}$
7	$\langle R_{\text{proj } \boldsymbol{u}}, Z^h \beta^h \rangle_{\Gamma_I}$	N/A	$-2.6E{-2}$	$8.0E{-3}$
8	$\mathcal{QE}_{\boldsymbol{u}_L}(\Pi_L^h \boldsymbol{\phi}_L^h)$	N/A	$-2.1E{-2}$	$-2.0E{-2}$
9	$QE_{\boldsymbol{u}_R}(\Pi_R^h \boldsymbol{\phi}_R^h)$	N/A	$-8.6E{-4}$	$-7.9E{-4}$
Res total		$-2.3E{-3}$	$-6.2E{-2}$	$-3.4E{-2}$
1	$(\Delta \boldsymbol{R}_{\boldsymbol{u}_L}, \Pi_L^h \boldsymbol{\phi}_L^h)$	$1.1E{-16}$	$4.1E{-4}$	$2.6E{-5}$
2	$(\Delta \boldsymbol{R}_{\boldsymbol{u}_R}, \Pi_R^h \boldsymbol{\phi}_R^h)$	$2.8E{-16}$	$-5.0E{-5}$	$-1.7E{-6}$
3	$(\Delta R_{p_L}, P_L^h \zeta_L^h)$	$-5.7E{-4}$	$2.4E{-2}$	$1.3E{-3}$
4	$(\Delta R_{p_R}, P_R^h \zeta_R^h)$	$-6.0E{-4}$	$7.8E{-3}$	$2.1E{-4}$
5	$\langle \Delta R_\xi, Z_h \beta^h \rangle_{\Gamma_I}$	$1.6E{-17}$	$-2.7E{-2}$	$-1.4E{-3}$
6	$\langle \Delta R_{\text{proj } p}, \boldsymbol{n} \cdot \Pi_L^h \boldsymbol{\phi}_L^h \rangle_{\Gamma_I}$	N/A	$1.1E{-3}$	$2.3E{-5}$
7	$\langle \Delta R_{\text{proj } \boldsymbol{u}}, Z^h \beta^h \rangle_{\Gamma_I}$	N/A	$2.7E{-2}$	$1.4E{-3}$
8	$\Delta \mathcal{QE}_{\boldsymbol{u}_L}(\Pi_L^h \boldsymbol{\phi}_L^h)$	N/A	$-1.5E{-3}$	$-4.9E{-5}$
9	$\Delta QE_{\boldsymbol{u}_R}(\Pi_R^h \boldsymbol{\phi}_R^h)$	N/A	$5.0E{-5}$	$1.7E{-6}$
Iterative total		$-1.2E{-3}$	$3.2E{-2}$	$1.5E{-3}$
Overall total		$-3.5E{-3}$	$-3.0E{-2}$	$-3.3E{-2}$
Conv. rate		.74	.89	.71
$\text{ratio}_{\text{proj}}$		N/A	6.5	5.1
$\text{ratio}_{\text{quad}}$		N/A	3.9	3.8

$$
\begin{aligned}
&+ \int_0^T (\dot{e}_{p_L}, \zeta_L)\,\mathrm{d}t + \int_0^T (e_{p_L}, -g_L'\widehat{(p_L, p_L^h)}\zeta_L)\,\mathrm{d}t + \int_0^T (\boldsymbol{e}_{\boldsymbol{u}_R}, a^{-1}\boldsymbol{\phi}_R)\,\mathrm{d}t + \int_0^T (\nabla \cdot \boldsymbol{e}_{\boldsymbol{u}_R}, \zeta_R)\,\mathrm{d}t \\
&+ \int_0^T \langle \boldsymbol{n} \cdot \boldsymbol{e}_{\boldsymbol{u}_R}, \beta \rangle_{\Gamma_I}\,\mathrm{d}t - \int_0^T (e_{p_R}, \nabla \cdot \boldsymbol{\phi}_R)\,\mathrm{d}t + \int_0^T (\dot{e}_{p_R}, \zeta_R)\,\mathrm{d}t \\
&+ \int_0^T (e_{p_R}, -g_R'\widehat{(p_R, p_R^h)}\zeta_R)\,\mathrm{d}t + \int_0^T \langle e_\xi, \boldsymbol{n} \cdot (\boldsymbol{\phi}_L - \boldsymbol{\phi}_R) \rangle_{\Gamma_I}\,\mathrm{d}t.
\end{aligned}
$$

Now we use (2.6) since e_p is potentially discontinuous, obtaining

$$
\begin{aligned}
\mathcal{E} = &\int_0^T (\boldsymbol{e}_{\boldsymbol{u}_L}, a^{-1}\boldsymbol{\phi}_L)\,\mathrm{d}t + \int_0^T (\nabla \cdot \boldsymbol{e}_{\boldsymbol{u}_L}, \zeta_L)\,\mathrm{d}t - \int_0^T \langle \boldsymbol{n} \cdot \boldsymbol{e}_{\boldsymbol{u}_L}, \beta \rangle_{\Gamma_I}\,\mathrm{d}t - \int_0^T (e_{p_L}, \nabla \cdot \boldsymbol{\phi}_L)\,\mathrm{d}t \\
&+ \sum_{k=1}^{k_L} \int_{t_{k-1}^+}^{t_k^-} (\dot{e}_{p_L}, \zeta_L)\,\mathrm{d}t + \sum_{k=1}^{k_L} ([e_{p_{L,k-1}}], \zeta_{L,k-1}) + \int_0^T (e_{p_L}, -g_L'\widehat{(p_L, p_L^h)}\zeta_L)\,\mathrm{d}t \\
&+ \int_0^T (\boldsymbol{e}_{\boldsymbol{u}_R}, a^{-1}\boldsymbol{\phi}_R)\,\mathrm{d}t + \int_0^T (\nabla \cdot \boldsymbol{e}_{\boldsymbol{u}_R}, \zeta_R)\,\mathrm{d}t + \int_0^T \langle \boldsymbol{n} \cdot \boldsymbol{e}_{\boldsymbol{u}_R}, \beta \rangle_{\Gamma_I}\,\mathrm{d}t - \int_0^T (e_{p_R}, \nabla \cdot \boldsymbol{\phi}_R)\,\mathrm{d}t
\end{aligned} \tag{5.1}
$$

Table 9

Error contributions for the short time period test with one iteration per Newton step and five Newton steps per composite time step.

Term		MFE	GFV (linear)	GFV (constant)
1	$(\boldsymbol{R}_{\boldsymbol{u}_L}, \boldsymbol{\phi}_L^h - \Pi_L^h \boldsymbol{\phi}_L^h)$	$-5.5E{-}3$	$-3.5E{-}3$	$-3.4E{-}3$
2	$(\boldsymbol{R}_{\boldsymbol{u}_R}, \boldsymbol{\phi}_R^h - \Pi_R^h \boldsymbol{\phi}_R^h)$	$-1.9E{-}4$	$-1.9E{-}4$	$-2.1E{-}4$
3	$(R_{p_L}, \zeta_L^h - P_L^h \zeta_L^h)$	$1.7E{-}3$	$1.4E{-}3$	$1.4E{-}3$
4	$(R_{p_R}, \zeta_R^h - P_R^h \zeta_R^h)$	$3.3E{-}4$	$3.1E{-}4$	$3.2E{-}4$
5	$\langle R_\xi, \beta^h - Z_h \beta^h \rangle_{\Gamma_I}$	$1.2E{-}17$	$2.0E{-}3$	$8.8E{-}4$
6	$\langle R_{\text{proj } p}, \boldsymbol{n} \cdot \Pi_L^h \boldsymbol{\phi}_L^h \rangle_{\Gamma_I}$	N/A	$-8.7E{-}3$	$-1.9E{-}2$
7	$\langle R_{\text{proj } \boldsymbol{u}}, Z^h \beta^h \rangle_{\Gamma_I}$	N/A	$1.2E{-}1$	$5.2E{-}2$
8	$\mathcal{QE}_{\boldsymbol{u}_L}(\Pi_L^h \boldsymbol{\phi}_L^h)$	N/A	$-2.5E{-}2$	$-2.1E{-}2$
9	$QE_{\boldsymbol{u}_R}(\Pi_R^h \boldsymbol{\phi}_R^h)$	N/A	$-6.9E{-}4$	$-7.4E{-}4$
Res total		$-3.6E{-}3$	$8.3E{-}2$	$9.7E{-}3$
1	$(\Delta \boldsymbol{R}_{\boldsymbol{u}_L}, \Pi_L^h \boldsymbol{\phi}_L^h)$	$5.6E{-}17$	$-1.3E{-}3$	$-6.7E{-}4$
2	$(\Delta \boldsymbol{R}_{\boldsymbol{u}_R}, \Pi_R^h \boldsymbol{\phi}_R^h)$	$1.7E{-}16$	$1.2E{-}4$	$4.6E{-}5$
3	$(\Delta R_{p_L}, P_L^h \zeta_L^h)$	$-1.3E{-}2$	$-1.0E{-}1$	$-3.9E{-}2$
4	$(\Delta R_{p_R}, P_R^h \zeta_R^h)$	$-1.4E{-}2$	$-7.0E{-}3$	$-4.6E{-}3$
5	$\langle \Delta R_\xi, Z_h \beta^h \rangle_{\Gamma_I}$	$-9.4E{-}17$	$1.2E{-}1$	$4.3E{-}2$
6	$\langle \Delta R_{\text{proj } p}, \boldsymbol{n} \cdot \Pi_L^h \boldsymbol{\phi}_L^h \rangle_{\Gamma_I}$	N/A	$-9.9E{-}4$	$-5.7E{-}4$
7	$\langle \Delta R_{\text{proj } \boldsymbol{u}}, Z^h \beta^h \rangle_{\Gamma_I}$	N/A	$-1.2E{-}1$	$-4.3E{-}2$
8	$\Delta \mathcal{QE}_{\boldsymbol{u}_L}(\Pi_L^h \boldsymbol{\phi}_L^h)$	N/A	$2.3E{-}3$	$1.2E{-}3$
9	$\Delta QE_{\boldsymbol{u}_R}(\Pi_R^h \boldsymbol{\phi}_R^h)$	N/A	$-1.2E{-}4$	$-4.6E{-}5$
Iterative total		$-2.7E{-}2$	$-1.1E{-}1$	$-4.3E{-}2$
Overall total		$-3.1E{-}2$	$-2.9E{-}2$	$-3.4E{-}2$
Conv. rate		.74	.89	.71
$\text{ratio}_{\text{proj}}$		N/A	17.0	11.4
$\text{ratio}_{\text{quad}}$		N/A	3.5	3.5

$$+ \sum_{k=1}^{k_R} \int_{t_{k-1}^+}^{t_k^-} (\dot{e}_{p_R}, \zeta_R)\,\mathrm{d}t + \sum_{k=1}^{k_R} ([e_{p_{R,k-1}}], \zeta_{R,k-1}) + \int_0^T (e_{p_R}, -\widehat{g_R'(p_R, p_R^h)}\zeta_R)\,\mathrm{d}t$$
$$+ \int_0^T \langle e_\xi, \boldsymbol{n} \cdot (\boldsymbol{\phi}_L - \boldsymbol{\phi}_R) \rangle_{\Gamma_I}\,\mathrm{d}t.$$

Expanding the errors, e.g., $e_{p_L} = p_L - p_L^h$, etc., using $\widehat{g'(p, p^h)} e_p = g(p) - g(p^h)$, and subtracting the equations in weak form

$$\int_0^T (a_L^{-1} \boldsymbol{u}_L, \boldsymbol{\phi}_L)\,\mathrm{d}t - \int_0^T (p_L, \nabla \cdot \boldsymbol{\phi}_L)\,\mathrm{d}t + \int_0^T \langle \xi, \boldsymbol{n} \cdot \boldsymbol{\phi}_L \rangle_{\Gamma_I}\,\mathrm{d}t + \int_0^T \langle d_L, \boldsymbol{n} \cdot \boldsymbol{\phi}_L \rangle_{\Gamma_L}\,\mathrm{d}t$$
$$+ \sum_{k=1}^{k_L} \int_{t_{k-1}^+}^{t_k^-} (\dot{p}_L, \zeta_L)\,\mathrm{d}t + \sum_{k=1}^{k_L} ([p_{L,k-1}], \zeta_{L,k-1}) + \int_0^T (\nabla \cdot \boldsymbol{u}_L, \zeta_L)\,\mathrm{d}t - \int_0^T (f_L, \zeta_L)\,\mathrm{d}t$$
$$- \int_0^T (g_L(p_L), \zeta_L)\,\mathrm{d}t + \int_0^T (a_R^{-1} \boldsymbol{u}_R, \boldsymbol{\phi}_R)\,\mathrm{d}t - \int_0^T (p_R, \nabla \cdot \boldsymbol{\phi}_R)\,\mathrm{d}t - \int_0^T \langle \xi, \boldsymbol{n} \cdot \boldsymbol{\phi}_R \rangle_{\Gamma_I}\,\mathrm{d}t$$
$$+ \int_0^T \langle d_R, \boldsymbol{n} \cdot \boldsymbol{\phi}_R \rangle_{\Gamma_R}\,\mathrm{d}t + \sum_{k=1}^{k_R} \int_{t_{k-1}^+}^{t_k^-} (\dot{p}_R, \zeta_R)\,\mathrm{d}t$$

Table 10

Error contributions for the long time period computation with three iterations per Newton step and five Newton steps per composite time step.

Term		MFE	GFV (linear)	GFV (constant)
1	$(\boldsymbol{R}_{\boldsymbol{u}_L}, \boldsymbol{\phi}_L^h - \Pi_L^h \boldsymbol{\phi}_L^h)$	$4.1E{-3}$	$-7.6E{-3}$	$-7.4E{-3}$
2	$(\boldsymbol{R}_{\boldsymbol{u}_R}, \boldsymbol{\phi}_R^h - \Pi_R^h \boldsymbol{\phi}_R^h)$	$1.4E{-4}$	$-1.3E{-4}$	$-1.0E{-4}$
3	$(R_{p_L}, \zeta_L^h - P_L^h \zeta_L^h)$	$-8.3E{-4}$	$-4.4E{-4}$	$-4.6E{-4}$
4	$(R_{p_R}, \zeta_R^h - P_R^h \zeta_R^h)$	$2.7E{-6}$	$3.0E{-5}$	$2.9E{-5}$
5	$\langle R_\xi, \beta^h - Z_h \beta^h \rangle_{\Gamma_I}$	$-1.6E{-17}$	$-1.1E{-3}$	$4.7E{-4}$
6	$\langle R_{\text{proj } p}, \boldsymbol{n} \cdot \Pi_L^h \boldsymbol{\phi}_L^h \rangle_{\Gamma_I}$	N/A	$-2.6E{-2}$	$-4.8E{-2}$
7	$\langle R_{\text{proj } \boldsymbol{u}}, Z^h \beta^h \rangle_{\Gamma_I}$	N/A	$-7.5E{-2}$	$3.2E{-2}$
8	$\mathcal{QE}_{\boldsymbol{u}_L}(\Pi_L^h \boldsymbol{\phi}_L^h)$	N/A	$-2.2E{-1}$	$-2.1E{-1}$
9	$QE_{\boldsymbol{u}_R}(\Pi_R^h \boldsymbol{\phi}_R^h)$	N/A	$-4.0E{-3}$	$-3.8E{-3}$
Res total		$3.4E{-3}$	$-3.3E{-1}$	$-2.4E{-1}$
1	$(\Delta \boldsymbol{R}_{\boldsymbol{u}_L}, \Pi_L^h \boldsymbol{\phi}_L^h)$	$3.3E{-16}$	$7.9E{-3}$	$3.1E{-4}$
2	$(\Delta \boldsymbol{R}_{\boldsymbol{u}_R}, \Pi_R^h \boldsymbol{\phi}_R^h)$	$1.6E{-15}$	$-5.2E{-6}$	$-7.0E{-7}$
3	$(\Delta R_{p_L}, P_L^h \zeta_L^h)$	$-1.9E{-3}$	$6.9E{-2}$	$3.9E{-3}$
4	$(\Delta R_{p_R}, P_R^h \zeta_R^h)$	$-1.9E{-3}$	$2.5E{-2}$	$7.1E{-4}$
5	$\langle \Delta R_\xi, Z_h \beta^h \rangle_{\Gamma_I}$	$-4.9E{-16}$	$-7.5E{-2}$	$-4.2E{-3}$
6	$\langle \Delta R_{\text{proj } p}, \boldsymbol{n} \cdot \Pi_L^h \boldsymbol{\phi}_L^h \rangle_{\Gamma_I}$	N/A	$2.2E{-3}$	$3.7E{-5}$
7	$\langle \Delta R_{\text{proj } \boldsymbol{u}}, Z^h \beta^h \rangle_{\Gamma_I}$	N/A	$7.5E{-2}$	$4.2E{-3}$
8	$\Delta \mathcal{QE}_{\boldsymbol{u}_L}(\Pi_L^h \boldsymbol{\phi}_L^h)$	N/A	$-1.0E{-2}$	$-3.5E{-4}$
9	$\Delta QE_{\boldsymbol{u}_R}(\Pi_R^h \boldsymbol{\phi}_R^h)$	N/A	$5.2E{-6}$	$7.0E{-7}$
Iterative total		$-3.9E{-3}$	$9.4E{-2}$	$4.6E{-3}$
Overall total		$-4.5E{-4}$	$-2.4E{-1}$	$-2.3E{-1}$
Conv. rate		.74	.89	.71
$\text{ratio}_{\text{proj}}$		N/A	10.9	9.4
$\text{ratio}_{\text{quad}}$		N/A	24.3	25.2

$$+ \sum_{k=1}^{k_R} ([p_{R,k-1}], \zeta_{R,k-1}) + \int_0^T (\nabla \cdot \boldsymbol{u}_R, \zeta_R)\, \mathrm{d}t - \int_0^T (f_R, \zeta_R)\, \mathrm{d}t - \int_0^T (g_R(p_R), \zeta_R)\, \mathrm{d}t$$
$$- \int_0^T \langle \boldsymbol{n} \cdot (\boldsymbol{u}_L - \boldsymbol{u}_R), \beta \rangle_{\Gamma_I}\, \mathrm{d}t = 0,$$

which are obtained by substituting the adjoint solutions as test functions in (2.5), gives

(5.2)
$$\mathcal{E} = -\int_0^T (a_L^{-1} \boldsymbol{u}_L^h, \boldsymbol{\phi}_L)\, \mathrm{d}t + \int_0^T (p_L^h, \nabla \cdot \boldsymbol{\phi}_L)\, \mathrm{d}t - \int_0^T \langle d_L, \boldsymbol{n} \cdot \boldsymbol{\phi}_L \rangle_{\Gamma_L}\, \mathrm{d}t - \int_0^T \langle \xi^h, \boldsymbol{n} \cdot \boldsymbol{\phi}_L \rangle_{\Gamma_I}\, \mathrm{d}t$$
$$+ \int_0^T (f_L, \zeta_L)\, \mathrm{d}t - \int_0^T (\nabla \cdot \boldsymbol{u}_L^h, \zeta_L)\, \mathrm{d}t - \sum_{k=1}^{k_L} \int_{t_{k-1}^+}^{t_k^-} (\dot{p}_L^h, \zeta_L)\, \mathrm{d}t - \sum_{k=1}^{k_L} ([p_{L,k-1}^h], \zeta_{L,k-1})$$
$$+ \int_0^T (g_L(p_L^h), \zeta_L)\, \mathrm{d}t - \int_0^T (a_R^{-1} \boldsymbol{u}_R^h, \boldsymbol{\phi}_R)\, \mathrm{d}t + \int_0^T (p_R^h, \nabla \cdot \boldsymbol{\phi}_R)\, \mathrm{d}t - \int_0^T \langle d_R, \boldsymbol{n} \cdot \boldsymbol{\phi}_R \rangle_{\Gamma_R}\, \mathrm{d}t$$
$$+ \int_0^T \langle \xi^h, \boldsymbol{n} \cdot \boldsymbol{\phi}_R \rangle_{\Gamma_I}\, \mathrm{d}t + \int_0^T (f_R, \zeta_R)\, \mathrm{d}t - \int_0^T (\nabla \cdot \boldsymbol{u}_R^h, \zeta_R)\, \mathrm{d}t - \sum_{k=1}^{k_R} \int_{t_{k-1}^+}^{t_k^-} (\dot{p}_R^h, \zeta_R)\, \mathrm{d}t$$

$$-\sum_{k=1}^{k_R}([p^h_{R,k-1}],\zeta_{R,k-1})+\int_0^T(g_R(p^h_R),\zeta_R)\,\mathrm{d}t+\int_0^T\langle\boldsymbol{n}\cdot(\boldsymbol{u}^h_L-\boldsymbol{u}^h_R),\beta\rangle_{\Gamma_I}\,\mathrm{d}t.$$

Taking into account that the divergence theorem implies

$$\begin{aligned}\int_0^T(\boldsymbol{R}_{\boldsymbol{u}_L},\boldsymbol{\phi}_L)\,\mathrm{d}t&=-\int_0^T(a_L^{-1}\boldsymbol{u}^h_L,\boldsymbol{\phi}_L)\,\mathrm{d}t+\int_0^T(p^h_L,\nabla\cdot\boldsymbol{\phi}_L)\,\mathrm{d}t\\&\quad-\int_0^T\langle d_L,\boldsymbol{n}\cdot\boldsymbol{\phi}_L\rangle_{\Gamma_D}\,\mathrm{d}t-\int_0^T\langle\xi^h,\boldsymbol{n}\cdot\boldsymbol{\phi}_L\rangle_{\Gamma_I}\,\mathrm{d}t,\int_0^T(\boldsymbol{R}_{\boldsymbol{u}_R},\boldsymbol{\phi}_R)\,\mathrm{d}t\\&=-\int_0^T(a_R^{-1}\boldsymbol{u}^h_R,\boldsymbol{\phi}_R)\,\mathrm{d}t+\int_0^T(p^h_R,\nabla\cdot\boldsymbol{\phi}_R)\,\mathrm{d}t\\&\quad-\int_0^T\langle d_R,\boldsymbol{n}\cdot\boldsymbol{\phi}_R\rangle_{\Gamma_D}\,\mathrm{d}t+\int_0^T\langle\xi^h,\boldsymbol{n}\cdot\boldsymbol{\phi}_R\rangle_{\Gamma_I}\,\mathrm{d}t,\end{aligned}$$

and that (2.6) implies

$$\begin{aligned}\int_0^T(R_p,\zeta)\,\mathrm{d}t&=\int_0^T(f,\zeta)\,\mathrm{d}t+\int_0^T(g(p^h),\zeta)\,\mathrm{d}t-\int_0^T(\nabla\cdot\boldsymbol{u}^h,\zeta)\,\mathrm{d}t\\&\quad-\sum_{k=1}^n\int_{t_{k-1}^+}^{t_k^-}(\dot{p}^h,\zeta)\,\mathrm{d}t-\sum_{k=1}^n([p^h_{k-1}],\zeta_{k-1}),\end{aligned}$$

we can rewrite (5.2) as

(5.3)
$$\mathcal{E}=\int_0^T(\boldsymbol{R}_{\boldsymbol{u}_L},\boldsymbol{\phi}_L)\,\mathrm{d}t+\int_0^T(R_{p_L},\zeta_L)\,\mathrm{d}t+\int_0^T(\boldsymbol{R}_{\boldsymbol{u}_R},\boldsymbol{\phi}_R)\,\mathrm{d}t+\int_0^T(R_{p_R},\zeta_R)\,\mathrm{d}t+\int_0^T\langle R_\xi,\beta\rangle_{\Gamma_I}\,\mathrm{d}t.$$

The discrete weak form implies the Galerkin orthogonality relationship

$$\begin{aligned}&\int_0^T(\boldsymbol{R}_{\boldsymbol{u}_L},\Pi^h_L\boldsymbol{\phi}_L)_Q\,\mathrm{d}t+\int_0^T(R_{p_L},P^h_L\zeta_L)_Q\,\mathrm{d}t+\int_0^T(\boldsymbol{R}_{\boldsymbol{u}_R},\Pi^h_R\boldsymbol{\phi}_R)_Q\,\mathrm{d}t\\&\qquad+\int_0^T(R_{p_R},P^h_R\zeta_R)_Q\,\mathrm{d}t+\int_0^T\langle R_\xi,Z_h\beta\rangle_{\Gamma_{I_Q}}\,\mathrm{d}t=0,\end{aligned}$$

where the subscript Q indicates the use of quadrature. Using the definitions in (3.7), we can rewrite this as

$$\begin{aligned}&\int_0^T(\boldsymbol{R}_{\boldsymbol{u}_L},\Pi^h_L\boldsymbol{\phi}_L)\,\mathrm{d}t+\int_0^T(R_{p_L},P^h_L\zeta_L)\,\mathrm{d}t+\int_0^T(\boldsymbol{R}_{\boldsymbol{u}_R},\Pi^h_R\boldsymbol{\phi}_R)\,\mathrm{d}t\\&\quad+\int_0^T(R_{p_R},P^h_R\zeta_R)\,\mathrm{d}t+\int_0^T\langle R_\xi,Z_h\beta\rangle_{\Gamma_I}\,\mathrm{d}t-QE_{\boldsymbol{u}_L}(\Pi^h_L\boldsymbol{\phi}_L)-QE_{p_L}(P^h_L\zeta_L)\\&\qquad-QE_{\boldsymbol{u}_R}(\Pi^h_R\boldsymbol{\phi}_R)-QE_{p_R}(P^h_R\zeta_R)-QE_\xi(Z^h\beta)=0.\end{aligned}\tag{5.4}$$

Finally, we subtract (5.4) from (5.3) to obtain (3.9).

5.2. Proof of Theorem 3.2. Before the Galerkin orthogonality terms are introduced, the estimates in section 5.1 are independent of the discretization. In particular, (5.3) applies to the geometrically coupled finite volume method. We introduce the appropriate Galerkin orthogonality expression

$$\begin{aligned}
&\int_0^T (\boldsymbol{R}_{\boldsymbol{u}_L}, \Pi_L^h \boldsymbol{\phi}_L)_Q \,\mathrm{d}t - \int_0^T \langle P_{R\to L}(p_R^h) - \xi^h, \boldsymbol{n}\cdot \Pi_L^h \boldsymbol{\phi}_L\rangle_{\Gamma_{I_Q}} \,\mathrm{d}t \\
&+ \int_0^T (R_{p_L}, P_L^h \zeta_L)_Q \,\mathrm{d}t + \int_0^T (\boldsymbol{R}_{\boldsymbol{u}_R}, \Pi_R^h \boldsymbol{\phi}_R)_Q \,\mathrm{d}t + \int_0^T (R_{p_R}, P_R^h \zeta_R)_Q \,\mathrm{d}t \\
&+ \int_0^T \langle R_\xi, Z_h \beta\rangle_{\Gamma_{I_Q}} \,\mathrm{d}t - \int_0^T \langle \boldsymbol{n}\cdot \boldsymbol{u}_L^h - P_{L\to R}(p_L^h), Z^h\beta\rangle_{\Gamma_{I_Q}} \,\mathrm{d}t = 0,
\end{aligned}$$

where the subscript Q indicates the use of quadrature. Using the definitions (3.7) and (3.8) we can rewrite this as

$$\begin{aligned}
(5.5)\ &\int_0^T (\boldsymbol{R}_{\boldsymbol{u}_L}, \Pi_L^h \boldsymbol{\phi}_L) \,\mathrm{d}t - \int_0^T \langle R_{\text{proj } p}, \boldsymbol{n}\cdot \Pi_L^h \boldsymbol{\phi}_L\rangle_{\Gamma_I} \,\mathrm{d}t + \int_0^T (R_{p_L}, P_L^h \zeta_L) \,\mathrm{d}t \\
&+ \int_0^T (\boldsymbol{R}_{\boldsymbol{u}_R}, \Pi_R^h \boldsymbol{\phi}_R) \,\mathrm{d}t + \int_0^T (R_{p_R}, P_R^h \zeta_R) \,\mathrm{d}t + \int_0^T \langle R_\xi, Z_h\beta\rangle_{\Gamma_I} \,\mathrm{d}t - \int_0^T \langle R_{\text{proj } \boldsymbol{u}}, Z^h\beta\rangle_{\Gamma_I} \,\mathrm{d}t \\
&- \mathcal{QE}_{\boldsymbol{u}_L}(\Pi_L^h \boldsymbol{\phi}_L) - QE_{p_L}(P_L^h \zeta_L) - QE_{\boldsymbol{u}_R}(\Pi_R^h \boldsymbol{\phi}_R) - QE_{p_R}(P_R^h \zeta_R) - \mathcal{QE}_\xi(Z^h\beta) = 0.
\end{aligned}$$

We subtract (5.5) from (5.3) to obtain (3.10).

5.3. Proofs of Theorems 3.3 and 3.4. The error estimate in (5.3) is valid for any discrete solution. However, once Galerkin orthogonality terms are added, the estimate becomes specific to the discretization, and the discrete solution must satisfy the relevant weak form for the estimate to be valid. Therefore, (5.4) and (5.5) and subsequent error estimates are only valid if the iterative solution method produces the exact discrete solution.

In the case of iterative solution of the discrete equations, we can express Galerkin orthogonality for the mortar method as

$$\begin{aligned}
(5.6)\ &\int_0^T (\boldsymbol{R}_{\boldsymbol{u}_L} - \Delta\boldsymbol{R}_{\boldsymbol{u}_L}, \Pi_L^h \boldsymbol{\phi}_L) \,\mathrm{d}t + \int_0^T (R_{p_L} - \Delta R_{p_L}, P_L^h \zeta_L) \,\mathrm{d}t \\
&+ \int_0^T (\boldsymbol{R}_{\boldsymbol{u}_R} - \Delta\boldsymbol{R}_{\boldsymbol{u}_R}, \Pi_R^h \boldsymbol{\phi}_R) \,\mathrm{d}t + \int_0^T (R_{p_R} - \Delta R_{p_R}, P_R^h \zeta_R) \,\mathrm{d}t + \int_0^T \langle R_\xi - \Delta R_\xi, Z_h\beta\rangle_{\Gamma_I} \,\mathrm{d}t \\
&- QE_{\boldsymbol{u}_L}(\Pi_L^h \boldsymbol{\phi}_L) - \Delta QE_{\boldsymbol{u}_L}(\Pi_L^h \boldsymbol{\phi}_L) - QE_{p_L}(P_L^h \zeta_L) - \Delta QE_{p_L}(P_L^h \zeta_L) \\
&- QE_{\boldsymbol{u}_R}(\Pi_R^h \boldsymbol{\phi}_R) - \Delta QE_{\boldsymbol{u}_R}(\Pi_R^h \boldsymbol{\phi}_R) - QE_{p_R}(P_R^h \zeta_R) - \Delta QE_{p_R}(P_R^h \zeta_R) \\
&- QE_\xi(Z^h\beta) - \Delta QE_\xi(Z^h\beta) = 0.
\end{aligned}$$

Equation (5.6) is a more general form of (5.4). A similar generalization of (5.5) can be constructed.

Therefore if iterative solution of the discrete equations results in an inexact approximate solution, the Δ terms in (5.6) must be appended to the right-hand sides of (3.9) and (3.10).

6. Conclusion. We consider two discretization techniques for solving coupled time-dependent nonlinear parabolic problems with different spatial and temporal scales that are posed on neighboring subdomains and are coupled through a common interface. The first, a mortar finite element method, provides a rigorously justified mechanism for coupling through the weak form. The second, a finite volume method, performs coupling via ad hoc techniques based on geometric considerations. We describe two iterative schemes for solving the discrete system of equations that arises at each time step. We then derive a posteriori error estimates for a specified quantity of interest which includes terms that account for the contributions to the error of various discretization choices. In particular, the estimates include terms quantifying the contributions to the error arising from solving the discrete equations for the approximation using only a finite number of iterations. We discuss the implementation of the a posteriori error estimates in detail. We conduct several numerical experiments that show that large error contributions associated with geometric projection may persist in time and that the error contribution resulting from inexact solution of the coupled systems of equations may be much larger than other contributions. We show by example that the chosen geometric coupling strategy has an impact on the convergence rate of the iterative method.

In the numerical solution of coupled systems, these results show that there a number of contributing factors that affect accuracy beyond mesh and time step selection. First, the choice of coupling method impacts not only the size of the discretization error but also the rate of convergence of the iterative solution technique. Second, the choice of iterative method and number of iterations performed can also contribute significantly to the error. Both of these effects can persist in time even for coupled parabolic problems.

REFERENCES

[1] T. Arbogast, L. C. Cowsar, M. F. Wheeler, and I. Yotov, *Mixed finite element methods on nonmatching multiblock grids*, SIAM J. Numer. Anal., 37 (2000), pp. 1295–1315.

[2] T. Arbogast, D. Estep, B. Sheehan, and S. Tavener, *A posteriori error estimates for mixed finite element and finite volume methods for problems coupled through a boundary with nonmatching grids*, IMA J. Numer. Anal., 34 (2014), pp. 1625–1653.

[3] T. Arbogast, G. Pencheva, M. F. Wheeler, and I. Yotov, *A multiscale mortar mixed finite element method*, Multiscale Model. Simul., 6 (2007), pp. 319–346.

[4] R. Becker and R. Rannacher, *An optimal control approach to a posteriori error estimation in finite element methods*, Acta Numer., 10 (2001), pp. 1–102.

[5] F. Ben Belgacem, *The mixed mortar finite element method for the incompressible Stokes problem: Convergence analysis*, SIAM J. Numer. Anal., 37 (2000), pp. 1085–1100.

[6] C. Bernardi, Y. Maday, and A. T. Patera, *A new nonconforming approach to domain decomposition: The mortar element method*, in Nonlinear Partial Differential Equations and Their Applications, Longman Scientific and Technical, Harlow, UK, 1994.

[7] C. Bernardi, Y. Maday, and F. Rapetti, *Basics and some applications of the mortar element method*, GAMM-Mitt., 28 (2005), pp. 97–123.

[8] F. Brezzi and M. Fortin, *Mixed and Hybrid Finite Element Methods*, Springer-Verlag, New York, 1991.

[9] T. Butler, D. Estep, and J. Sandelin, *A computational measure theoretic approach to inverse sensitivity problems* II: *A posteriori error analysis*, SIAM J. Numer. Anal., 50 (2012), pp. 22–45.

[10] J. R. Cary, J. Candy, R. H. Cohen, S. Krasheninnikov, D. C. McCune, D. J. Estep, J. Larson, A. D. Malony, A. Pankin, P. H. Worley, J. A. Carlsson, A. H. Hakim, P. Hamill, S. Kruger, M. Miah, S. Muzsala, A. Pletzer, S. Shasharina, D. Wade-Stein, N. Wang, S. Balay, L. McInnes, H. Zhang, T. Casper, L. Diachin, T. Epperly, T. D. Rognlien, M. R.

Fahey, J. Cobb, A. Morris, S. Shende, G. W. Hammett, K. Indireshkumar, D. Stotler, and A. Y. Pigarov, *First results from core-edge parallel composition in the facets project*, J. Phys.: Conf. Ser., 125 (2008), 012040.

[11] J. R. Cary, A. Hakim, M. Miah, S. Kruger, A. Pletzer, S. Shasharina, S. Vadlamani, A. Pankin, R. Cohen, T. Epperly, T, Rognlien, R. Groebner, S. Balay, L. McInnes, and H. Zhang, *FACETS — a framework for parallel coupling of fusion components*, in Proceedings of the 18th IEEE Euromicro International Conference on Parallel, Distributed and Network-Based Computing, Pisa, Italy, 2010, pp. 435–442.

[12] J. B. Collins, D. Estep, and S. Tavener, *A posteriori error analysis for finite element methods with projection operators as applied to explicit time integration techniques*, BIT, 2014, DOI 10.1007/s10543-014-0534-9.

[13] G. Edwards and C. Rogers, *Finite volume discretization with imposed flux continuity for the general tensor pressure equation*, Comput. Geosci., 2 (1998), pp. 259–290.

[14] D. Estep, *Error estimation for multiscale operator decomposition for multiphysics problems*, in Multiscale Methods: Bridging the Scales in Science and Engineering, J. Fish, ed., Oxford University Press, Oxford, UK, 2010.

[15] D. Estep, M. G. Larson, and R. D. Williams, *Estimating the error of numerical solutions of systems of reaction-diffusion equations*, Mem. Amer. Math. Soc., 146 (2000), 696.

[16] D. Estep, A. Målqvist, and S. Tavener, *Nonparametric density estimation for randomly perturbed elliptic problems* I: *Computational methods, a posteriori analysis, and adaptive error control*, SIAM J. Sci. Comput., 31 (2009), pp. 2935–2959.

[17] D. Estep, A. Målqvist, and S. Tavener, *Nonparametric density estimation for randomly perturbed elliptic problems* II: *Applications and adaptive modeling*, Internat. J. Numer. Methods Engrg., 80 (2009), pp. 846–867.

[18] D. Estep, M. Pernice, D. Pham, S. Tavener, and H. Wang, *A posteriori analysis of a cell-centered finite volume method for semilinear elliptic problems*, J. Comput. Appl. Math., 233 (2009), pp. 459–472.

[19] D. Estep, S. Tavener, and T. Wildey, *A posteriori analysis and improved accuracy for an operator decomposition solution of a conjugate heat transfer problem*, SIAM J. Numer. Anal., 46 (2008), pp. 2068–2089.

[20] D. Estep, S. Tavener, and T. Wildey, *A posteriori error analysis for a transient conjugate heat transfer problem*, Finite Elem. Anal. Des., 45 (2009), pp. 263–271.

[21] D. Estep, S. Tavener, and T. Wildey, *A posteriori error estimation and adaptive mesh refinement for a multi-discretization operator decomposition approach to fluid-solid heat transfer*, J. Comput. Phys., 229 (2010), pp. 4143–4158.

[22] C. Farhat, M. Lesoinne, and P. LeTallec, *Load and motion transfer algorithms for fluid/structure interaction problems with non-matching discrete interfaces: Momentum and energy conservation, optimal discretization and application to aeroelasticity*, Comput. Methods Appl. Mech. Engrg., 157 (1998), pp. 95–114.

[23] S. Gaiffe, R. Glowinski, and R. Masson, *Domain decomposition and splitting methods for mortar mixed finite element approximations to parabolic equations*, Numer. Math., 93 (2002), pp. 53–75.

[24] B. Ganis and I. Yotov, *Implementation of a mortar mixed finite element method using a multiscale flux basis*, Comput. Methods Appl. Mech. Engrg., 198 (2009), pp. 3989–3998.

[25] M. B. Giles and E. Suli, *Adjoint methods for PDEs: A posteriori error analysis and postprocessing by duality*, Acta Numer., 11 (2002), pp. 145–236.

[26] R. Glowinski and M. F. Wheeler, *Domain decomposition and mixed finite element methods for elliptic problems*, in First International Symposium on Domain Decomposition Methods for Partial Differential Equations, R. Glowinski, G. H. Golub, G. A. Meurant, and J. Periaux, eds., SIAM, Philadelphia, 1988, pp. 144–172.

[27] P. Hansbro and M. G. Larson, *A posteriori error estimates for continuous/discontinuous Galerkin approximations of the Kirchhoff-Love plate*, Comput. Methods Appl. Mech. Engrg., 200 (2011), pp. 3289–3295.

[28] T.-T.-P. Hoang, J. Jaffré, C. Japhet, M. Kern, and J. E. Roberts, *Space-time domain decomposition methods for diffusion problems in mixed formulations*, SIAM J. Numer. Anal., 51 (2013), pp.

3532–3559.

[29] D. E. Keyes, L. C. McInnes, C. Woodward, W. Gropp, E. Myra, M. Pernice, J. Bell, J. Brown, A. Clo, J. Connors, E. Constantinescu, D. Estep, K. Evans, C. Farhat, A. Hakim, G. Hammond, G. Hansen, J. Hill, T. Isaac, X. Jiao, K. Jordan, D. Kaushik, E. Kaxiras, A. Koniges, K. Lee, A. Lott, Q. Lu, J. Magerlein, R. Maxwell, M. McCourt, M. Mehl, R. Pawlowski, A. Peters Randles, D. Reynolds, B. Riviere, U. Ruede, T. Scheibe, J. Shadid, B. Sheehan, M. Shephard, A. Siegel, B. Smith, X. Tang, C. Wilson, and B. Wohlmuth, *Multiphysics simulations: Challenges and opportunities*, Int. J. High Perf. Comput. Appl., 27 (2013), pp. 4–83.

[30] A. Quarteroni, F. Pasquarelli, and A. Valli, *Heterogeneous domain decomposition: Principles, algorithms, applications*, in Fifth International Symposium on Domain Decomposition Methods for Partial Differential Equations, SIAM, Philadelphia, 1992, pp. 129–150.

[31] J. E. Roberts and J. Thomas, *Mixed and hybrid methods*, in Handbook of Numerical Analysis, Elsevier Science Publishers B.V., Amsterdam, 1991, pp. 523–639.

[32] T. Russell and M. F. Wheeler, *Finite element and finite difference methods for continuous flows in porous media*, in The Mathematics of Reservoir Simulation, R. E. Ewing, ed., SIAM, Philadelphia, 1984, pp. 35–106.

[33] A. Weiser and M. F. Wheeler, *On convergence of block-centered finite differences for elliptic problems*, SIAM J. Numer. Anal., 25 (1988), pp. 351–375.

[34] M. F. Wheeler and I. Yotov, *A posteriori error estimates for the mortar mixed finite element method*, SIAM J. Numer. Anal., 43 (2005), pp. 1021–1042.